Remote Sensing of Environment 236 (2020) 111454

Contents lists available at ScienceDirect

Remote Sensing of Environment

journal homepage: www.elsevier.com/locate/rse

Improving burn severity retrieval by integrating tree canopy cover into radiative transfer model simulation

Changming Yin[a], Binbin He[a,*], Marta Yebra[b,c,d], Xingwen Quan[a,**], Andrew C. Edwards[d,e], Xiangzhuo Liu[a], Zhanmang Liao[a]

[a] School of Resources and Environment, University of Electronic Science and Technology of China, Chengdu, Sichuan, 611731, China
[b] Fenner School of Environment and Society, Australian National University, Canberra, ACT, 2601, Australia
[c] Bushfire and Natural Hazards Cooperative Research Centre, East Melbourne, VIC, 3002, Australia
[d] Research School of Aerospace, Mechanical, and Environmental Engineering, Australian National University, Canberra, ACT, 2601, Australia
[e] Darwin Centre for Bushfire Research, Charles Darwin University, Darwin, NT, 0909, Australia

ARTICLE INFO

Keywords:
Burn severity
Tree canopy cover
FRT
Radiative transfer model
Sentinel-2A

ABSTRACT

Burn severity mapping greatly informs fire management and can be used to predict post-fire vegetation recovery. Satellite remote sensing is a cost-effective method for estimating burn severity, providing a comprehensive spatially explicit view of whole landscapes. However, the proportion of tree canopy cover (TCC) affects the reflectance signal, obscuring background char and ash. Consequently, traditional optical satellite remote sensing methods that do not account for variation in TCC misclassify burn severity, especially in areas with extremely low or high TCC. In this study, TCC data served to parameterize and constrain the inversion of the Forest Reflectance and Transmittance (FRT) radiative transfer model (RTM) to alleviate spectral confusion when retrieving burn severity. The methodology was evaluated using field measurements of burn severity for a series of wildfires in the fire-prone tropical savannas of northern Australia and the western United States. Burn severity classes were used for Australia while the Composite Burn Index (CBI) for US. Reflectance data from Sentinel-2A Multi-Spectral Instrument (MSI) and Landsat-5 Thematic Mapper (TM) corresponding to post-fire field survey dates were used to retrieve burn severity using FRT RTM (with and without using TCC information in its parameterization and inversion) and two standard empirical burn indices, dNBR and RdNBR, for comparison. Using FRT RTM without TCC constraint produced an overestimation for low burn severity in regions with low TCC and an underestimation for moderate and high burn severity in regions with high TCC. Burn severity estimation accuracy significantly improved by integrating TCC in the parameterization and inversion of FRT RTM. The overall accuracy in northern Australia increased from 65% to 81%, and the kappa coefficient increased from 0.35 to 0.55. In the western United States, R^2 between estimated and observed CBI, increased from 0.33 to 0.54, root mean square error (RMSE) reduced from 0.53 to 0.43, and in all instances, the method performed better than dNBR and RdNBR. The method used in this study achieved more accurate burn severity mapping, thus assisting land managers to better understand post-fire vegetation resilience and forest management.

1. Introduction

Wildfire is a major disturbance agent in terrestrial ecosystems worldwide, leading to changes in vegetation carbon stocks and influencing the temporal variability in carbon, water and energy fluxes (Bowman et al., 2009; Chuvieco, 2009; Flannigan et al., 2000). Burn severity is defined as the impact of fire on soil and vegetation in a given sampling area (Chuvieco et al., 2006; Edwards et al., 2013). Accurate measurement of burn severity is critical to quantifying fire impact on key ecological processes (e.g. tree mortality, post-fire recovery, and intra-species/inter-species competition), and essential for post-fire forest management activities (Frolking et al., 2009; Lentile et al., 2006).

Different approaches have been developed to evaluate burn severity, through field surveys and methods based on remote sensing. Field surveys are based on quantitative or qualitative assessments of post-fire soil and vegetation conditions. The Composite Burn Index

* Corresponding author. School of Resources and Environment, University of Electronic Science and Technology of China, Chengdu, Sichuan, 611731, China.
** Corresponding author. School of Resources and Environment, University of Electronic Science and Technology of China, Chengdu, Sichuan, 611731, China.
E-mail addresses: binbinhe@uestc.edu.cn (B. He), xingwen.quan@uestc.edu.cn (X. Quan).

https://doi.org/10.1016/j.rse.2019.111454
Received 19 June 2019; Received in revised form 5 September 2019; Accepted 30 September 2019
Available online 18 November 2019
0034-4257/

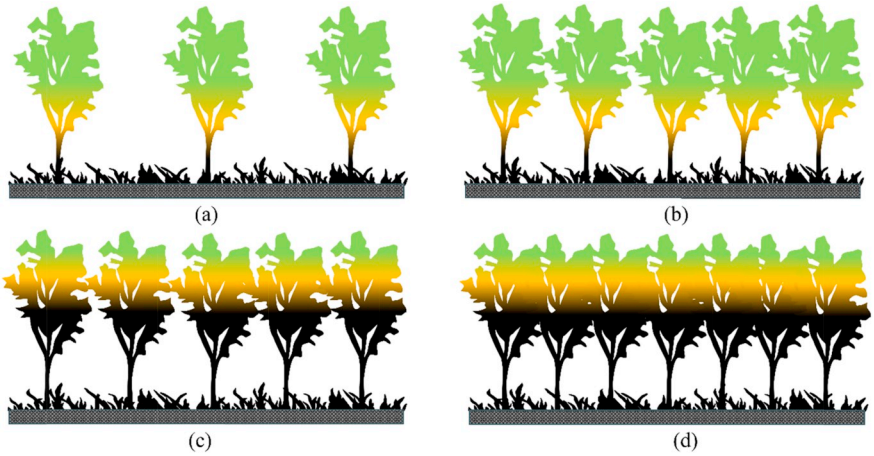

Fig. 1. Sketch map of the influence of tree canopy cover (TCC) on burn severity estimation from optical remote sensing techniques: (a) and (b) represent low burn severity with low and medium TCC, respectively; (c) and (d) represent medium burn severity with medium and high TCC, respectively. A lower TCC in (a) will result in an overestimation of burn severity while a higher TCC in (d) will result in an underestimation.

(CBI) (Key and Benson, 2006) and the GeoCBI (De Santis and Chuvieco, 2009) are common ground-based severity indices. CBI has continuous values ranging from 0 (unburned) to 3 (completely burned). GeoCBI is a modified version of CBI that computes the burn severity of a plot accounting for the fraction of cover (FCOV) of each vegetation strata. GeoCBI is, therefore, better adapted to remotely sensed data (De Santis and Chuvieco, 2009). However, GeoCBI has the risk of increasing the area of moderate and high burn severity in sparse tree covered area. Consider for example, a place where middle and lower shrubs and grasslands are dense but trees are sparse. If only the grasslands and shrubs are burned (while the upper trees are not), according to the criterion of GeoCBI, the burning ratio of grasslands and shrubs will occupy a higher weight for their higher fractional cover. GeoCBI will yield a high value when in fact the area belongs at a lower burn severity level.

In contrast to field survey methods, using remotely sensed data is much more cost-efficient and provides a comprehensive spatial coverage (Chuvieco, 2009; Chuvieco et al., 2007). The methods for burn severity estimation based on passive optical remote sensing techniques can be divided into four categories:

(i) Empirical statistical models. The most commonly used spectral indices include the Normalized Burn Ratio (NBR) (Roy et al., 2006), the differenced NBR (dNBR) (Miller and Thode, 2007), and the Relative dNBR (RdNBR) (Miller et al., 2009). Spectral indices have been widely used due to their simple calculation and spatially extensive applicability. However, they lack physical meaning, require extensive local calibration for accuracy, and do not make use of the full spectrum available (De Santis et al., 2010).

(ii) Spectral Mixture Analysis (SMA) methods. In these methods, post-fire burn severity is estimated by solving sub-pixel mixing (Fernandez-Manso et al., 2016b; Quintano et al., 2017; Quintano et al., 2013). An advantage is their use of all spectral bands from one single post-fire image (Sunderman and Weisberg, 2011), but this is limited by the need for an extensive, site-specific end-member library (Edwards et al., 2018).

(iii) Random forest regression. The random forest classifier has been found to be suited for burn severity mapping as it can consider multiple environmental variables simultaneously (Hultquist et al., 2014). However, classification accuracy strongly relies on the selection of the training data, and the classification results are generally site-specific (Collins et al., 2018).

(iv) Radiative transfer models (RTMs). RTMs are firstly 'forward' applied to simulate reflectance and transmittance at leaf and canopy levels corresponding to specific burn severity levels, expressed for example using CBI or GeoCBI. In a subsequent step, surface reflectance extracted from remotely sensed data is used to estimate the biophysical and biochemical variables of the vegetation that determined a certain CBI or GeoCBI value (De Santis et al. 2009, 2010). The model selected to simulate the reflectance should be sensitive to burn severity variations in different vegetation layers since CBI and GeoCBI scores consider five strata (Chuvieco et al., 2007). Chuvieco et al. (2006) initially used the Kuusk Markov Chain Canopy Reflectance Model (MCRM) (Kuusk, 1995) for burn severity estimation as this model considers two vegetation canopies. However, MCRM assumes a uniform turbid medium, which is not suitable over forested areas. In response, De Santis et al. (2009) suggested using the geometric RTM GeoSAIL model, which describes forest canopy closer to reality. RTM inversion methods have a better universality than empirical models, but RTM parameterization is challenging (Yebra et al., 2018).

For its continuous accessibility and its easy interpretation, we mainly focus on burn severity estimation using optical remote sensing data. Any of the previously presented methods that retrieve burn severity using a single optical post-fire satellite image share a limitation in that they increase the proportion of high burn severity classes in regions with low tree canopy cover (TCC), and underestimate burn severity in regions with dense tree canopy cover (Miller et al., 2009). Dead leaf litter and charcoal will have a different contribution to the signal received by remote sensing sensors with TCC variation. For example, given two plots with the same low burn severity (only understory vegetation burned) but different TCC level (Fig. 1a and b), the background char and dead litter will contribute more to the observed spectral signal for the plot with lower TCC (Fig. 1a) than for the plot with higher TCC (Fig. 1b). This will result in an overestimation of burn severity in the situation of lower TCC (Fig. 1a). Conversely, for plots with the same medium burn severity (Fig. 1c and d), if the TCC is extremely high (Fig. 1d), the spectral signal from the background will be obscured by the green tree canopy, leading to an underestimation of the burn severity. Therefore, the same burn severity could correspond to different spectral signatures and the same spectral signature could correspond to different levels of burn severity with the variation of TCC. Consequently, the proportion of TCC plays an important role in relating reflectance to burn severity, and thus should be considered in RTM parameterization and backward inversion, however, this issue has been not addressed in previous studies.

In this study, we aim to develop a more accurate RTM-based method to solve the errors in burn severity estimation caused by TCC variation by considering TCC in the parameterization and backward inversion of FRT RTM (RTM + TCC). The value of this approach is demonstrated when comparing the results to those obtained using the traditional RTM Global Optimal Search (RTM + GOS) method. Several fire-affected regions across northern Australia and in the western United States were

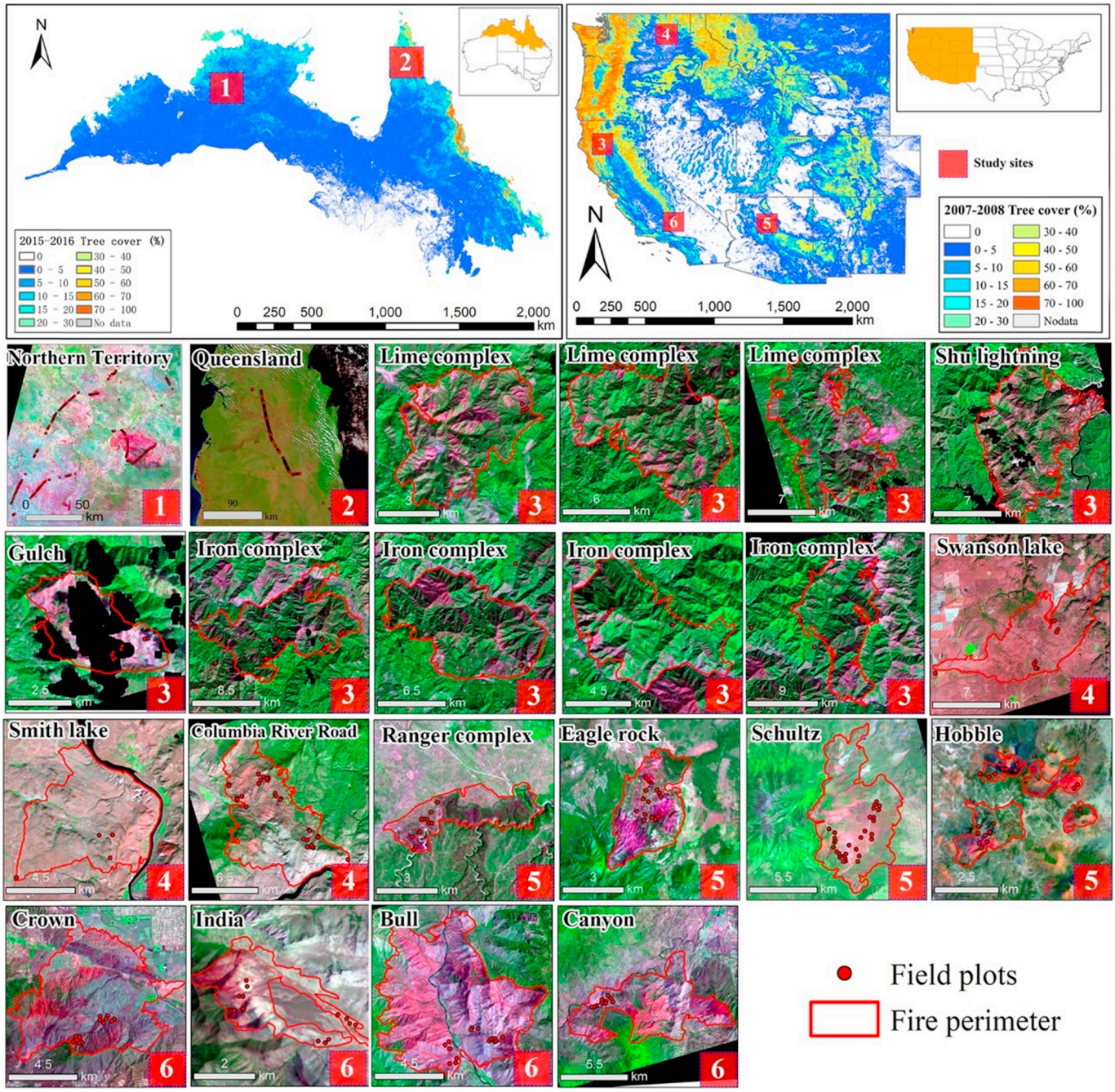

Fig. 2. Location of the six study sites and field plots. The background map used in the top two maps is the percent tree canopy cover (TCC) extracted from the MODIS Vegetation Continuous Fields product of 2015–2016 for northern Australia and 2007–2008 for the western United States. Image maps are false color composites (SWIR2, NIR, and red bands) of post-fire Sentinel-2A MSI (maps 1 and 2) and Landsat-5 TM (maps 3 to 6) and show the location of the field plots for each of the six study sites. The western United States fire perimeters were provided by the USGS Monitoring Trends in Burn Severity (MTBS) project. (For interpretation of the references to color in this figure legend, the reader is referred to the Web version of this article.)

selected to verify the validity and universality of the proposed method on solving spectral confusion errors in sparse and dense tree-covered areas.

2. Materials and methods

2.1. Study area and data sampling

Spectral confusion between burn severity levels generally occurs in regions with both sparse and dense tree canopy layers and leads to errors in burn severity mapping. We carefully selected our study areas to contain different vegetation types with very different TCC (northern Australia, sparse tree cover, and western United States, dense tree cover) to better test our methodology to reduce the influence of TCC variation on burn severity retrieval and comprehensively verify the validity and universality of our method. The first study area includes two study sites and is located in the tropical savannas of northern Australia (Fig. 2, Table 1). Australia's tropical savannas cover 1.9 million km^2, approximately 25% of the continent, and are comprised of open woodlands, woodlands and open forests (Edwards et al., 2018). Fires in northern Australia generally ignite during the dry season months (approximately May to October) with little or no rain, relatively

Table 1
List of fires in northern Australia and the western United States used in the study. Fire date represents the time when the fire started. TCC (%) is derived from the pre-fire MODIS Vegetation Continuous Fields product and represents the tree canopy cover range of the fire region.

Fire name	State	Fire date	Field survey date	Vegetation type	TCC (%)
Daly	Northern Territory	2016/08/21	2016/10/19	savanna	2–14
Victoria	Northern Territory	2016/09/01	2016/10/19	savanna	3–10
Elsey	Northern Territory	2016/10/01	2016/10/19	savanna	2–14
Cook	Queensland	2016/06/26	2016/07/27	savanna	2–34
Schultz	Arizona	2010/06/20	2011/08/01	coniferous forests	19–48
Ranger Complex	Arizona	2010/07/17	2011/08/03	coniferous forests	30–43
Eagle Rock	Arizona	2010/06/11	2011/07/30	coniferous forests	16–40
Hobble	Arizona	2010/08/30	2011/07/31	coniferous forests	9–25
Shu Lightning	California	2008/06/21	2009/10/31	coniferous forests	13–53
Iron Complex	California	2008/06/21	2009/11/01	coniferous forests	43–74
Lime Complex	California	2008/06/21	2009/11/01	coniferous forests	57–68
Gulch	California	2008/09/07	2009/11/01	savanna	15–34
Indian	California	2010/07/18	2011/08/13	open shrublands	2–11
Bull	California	2010/07/26	2011/08/14	savanna	3–18
Canyon	California	2010/09/12	2011/08/05	savanna	4–12
Crown	California	2010/07/29	2011/08/17	savanna	6–18
Swanson Lake	Washington	2008/08/18	2009/10/20	coniferous forests	2–20
Columbia River Road	Washington	2008/08/07	2009/10/22	coniferous forests	6–48
Smith Lake	Washington	2008/08/02	2009/10/23	savanna	2–4

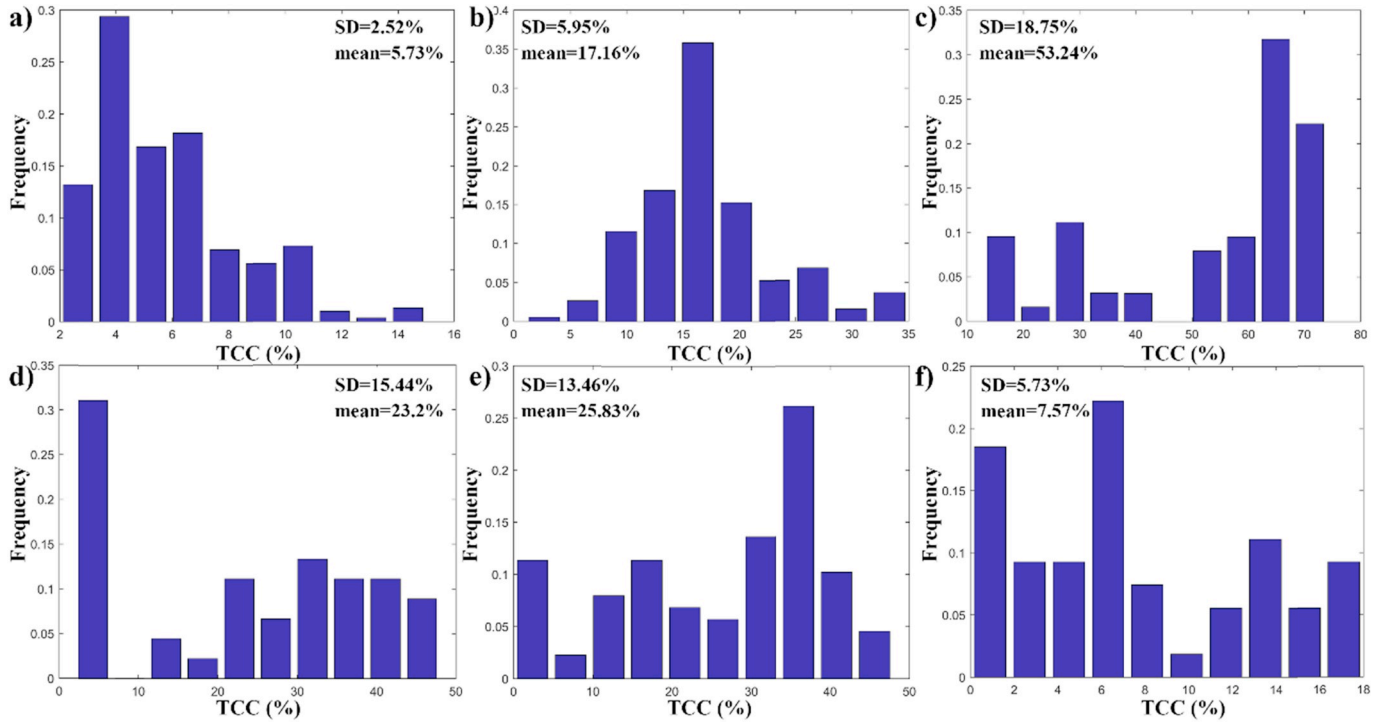

Fig. 3. Frequency distribution histograms of the pre-fire TCC (%) of the six study sites in northern Australia (a and b) and the western United States (c to f).

low humidity and high temperatures (Gill et al., 1996). The dry season months can be further separated into early dry season (EDS) (approximately May to July) and late dry season (LDS) (approximately August to October). Fires occurring during the EDS are patchier and less severe, while the LDS fires are more intense and severe (Edwards et al., 2018). Study site 1 experienced LDS (August to middle October 2016) fires while site 2 experienced EDS fires (June to late July 2016). Post-fire field sampling was carried out on about one-week after the fires (19 October 2016 and 27 July 2016 for sites 1 and 2, respectively), using the savanna rapid assessment technique of Edwards et al. (2013). The burn severity is classified into five categories considering the degree of charring and scorching of photosynthetic and non-photosynthetic plant material in the different strata: (a) PATCHY (small trees and shrubs scorched to 2 m, < 80% burnt ground layer patchiness); (b) LOW (small trees and shrubs scorched to 2 m, > 80% burnt ground layer patchiness); (c) MODERATE (scorched leaves through the mid-storey (> 2 and < 8 m) perhaps into the lower parts of the upper canopy); (d) HIGH (complete canopy scorch) and; (e) EXTREME (all foliage removed or charred). The burn severity of the two study sites in northern Australian savanna was classified into severe (SV) and not-severe (NSV) as simply differentiating "Severe" from "Not-Severe" fire-affected areas can provide adequate and more accurate information for fire management (Edwards et al. 2013, 2018).Conseqeutnly, the "patchy", "low" and "moderate" burnt level were merged as "NSV" burnt level while the "high" and "extreme" were merged as "SV" burnt level. There was a total of 303 (SV: 182; NSV: 121) and 179 (SV: 16; NSV: 163) field plots for study sites 1 and 2, respectively.

The second study area includes four study sites in the western United States (Fig. 2), including 15 fires that occurred across three states (Fig. 2, Table 1). The vegetation types in these four study sites is

comprised of deciduous and coniferous forests, savannas, shrublands, and grasslands. The field data of the western United States is a public dataset of the United States Department of Agriculture (USDA), which was funded by the Joint Fire Sciences Program (Addison and Oommen, 2018; Sikkink et al., 2013). The burn severity of these study sites was assessed using the CBI from 2009 to 2011 (about one-year post-fire). The fire perimeters of the western United States were provided by the Monitoring Trends in Burn Severity (MTBS, https://www.mtbs.gov/, last access 13/08/2019). MTBS is an interagency program whose goal is to consistently map the burn severity and extent of large fires across all lands of the United States from 1984 to the present. In this study, a total of 227 field plots were selected after removing non-tree plots and plots that appeared covered by cloud and cloud shadow in the corresponding satellite imagery.

The frequency distribution of percent TCC in the field plots of the six study sites was calculated (Fig. 3). In the two northern Australia study sites TCC is low, for example, TCC of the vast majority of study site 1 is less than 10%. The sparse tree distribution made it difficult to classify the burn severity. By contrast, TCC of the western United States study sites is much higher, with the highest TCC being in study site 3, where it reaches 70%.

2.2. Satellite data and processing

2.2.1. Reflectance data

The fires in the western United States were ignited from 2008 to 2010. Therefore, Landsat-5 Thematic Mapper (TM) data were used. In northern Australia, Sentinel-2A Multi-Spectral Instrument (MSI) data were preferred, for three main reasons: firstly, the acquisition dates of the Sentinel-2A MSI data were closer to the field survey time; secondly, the cloud cover was lower than in the Landsat-8 OLI imagery and; thirdly, compared to Landsat-5 TM, Sentinel-2A MSI provides information in three Vegetation Red Edge (VRE) bands that are suitable for discriminating burn severity (Fernández-Manso et al. 2016a).

The Sentinel-2A satellite carries a single MSI with 13 spectral channels in the visible/near infrared (VNIR) and shortwave infrared (SWIR) spectral range. In this study, nine spectral bands from the visible (VIS) to SWIR bands (bands 2–8a and bands 11 & 12) and post-fire NBR were used for estimating burn severity at the northern Australia tropical savanna study sites. Data were acquired for study site 1 and study site 2 on 24 October 2016 and 03 August 2016, respectively. The spatial resolution of the nine spectral bands was unified to 20 m. Sentinel-2A MSI data were downloaded from the Copernicus Open Access Hub (https://scihub.copernicus.eu/, last access 13/08/2019). The atmospheric correction of Sentinel-2A MSI data was implemented using the Sen2Cor Tool (version 2.3.1) (Gascon et al., 2017; Louis et al., 2016), converting Level-1C to Level-2A Bottom-of-Atmosphere (BOA) reflectance, using the Sen2Cor default parameters. Sen2Cor has two main modules, the Scene Classification (SCL) module and the Atmospheric Correction (AC) module (Main-Knorn et al., 2017). The AC is performed using a set of LUTs generated via libRadtran (Mayer and Kylling, 2005). In AC, the configuration parameters include: (1) aerosol type; (2) atmosphere type; (3) ozone content. Aerosol type can be selected as rural or maritime (the default is rural). There are 2 atmosphere types (mid-latitude summer or mid-latitude winter), which are selected automatically by Sen2Cor according to the scene geographic location and climatology (Main-Knorn et al., 2017). Ozone content is also selected automatically by Sen2Cor.

Landsat-5 TM surface reflectance and post-fire NBR data were used in the western United States. The surface reflectance product of Landsat-5 TM was downloaded from USGS Earth Explorer (https://earthexplorer.usgs.gov/, last access 13/08/2019) and generated from the Landsat Ecosystem Disturbance Adaptive Processing System (LEDAPS), specialized software originally developed through NASA's Making Earth System Data Records for Use in Research Environments (MEaSUREs) (Masek et al., 2006). The clouds and shadows of both Landsat-5 and Sentinel-2 data were detected and masked using the Fmask algorithm (Zhu et al., 2015; Zhu and Woodcock, 2012; Qiu et al., 2018). The pre and post-fire images were selected according to the fire ignition and field collection date.

2.2.2. MODIS Vegetation Continuous Fields data

The pre-fire TCC data should be as close as possible to the fire ignition date to accurately describe the TCC condition before fire. Therefore, the MOD44B Version 6 Vegetation Continuous Fields (VCF) product was used for its high temporal resolution compared with other TCC product. MODIS VCF is a global representation of surface vegetation cover as gradations of three ground cover components: percentage of tree cover, non-tree cover, and non-vegetated (bare) (Carroll et al., 2010). VCF products provide a continuous, quantitative description of land surface cover at 250 m spatial resolution, with a sub-pixel depiction of the percentage of cover of the three ground cover components (DiMiceli et al., 2011). VCF products were accessed from NASA Earthdata Search (https://search.earthdata.nasa.gov/, last access 13/08/2019). The TCC layer of one year before the different fires occurred was used to parameterize and constrain the RTM. MODIS VCF data of the two study areas were resampled to 20 m and 30 m to maintain uniform spatial resolution with Sentinel-2A MSI and Landsat-5 TM data, respectively, using nearest-neighbor interpolation. In future work we would explore the use of pre-fire TCC products with higher spatial resolution as auxiliary data to assess the influence of spatial resolution on the accuracy of burn severity estimation. The TCC maps show that the majority of the TCC of northern Australia tropical savannas is relatively low ($\leq$30%) while the TCC of the study sites in the western United States is higher (even over 70%) (Table 1, Fig. 3).

2.3. Retrieval of burn severity using FRT RTM

The methodology to retrieve burn severity is illustrated in Fig. 4. Four consecutive phases were carried out to estimate burn severity based on RTM: (i) model selection to simulate the reflectance corresponding to different burn severities; (ii) sensitivity analysis to ascertain the sensitive parameters for burn severity simulation; (iii) forward modeling, which includes the parameterization of the RTM based on the sensitivity analysis results and generation of the look-up table (LUT); and (iv) RTM model inversion by finding the simulated spectral reflectance spectrum (stored in the LUT) that best matches the observed spectrum using a merit function.

2.3.1. Model selection

FRT RTM (version 04.2013) (Kuusk and Nilson, 2000) was selected for burn severity estimation. FRT is a directional multispectral forest reflectance model in the optical domain of radiation 400–2400 nm with 1 nm spectral resolution. The model assumes that forest canopies consist of three layers: a discontinuous upper canopy of trees in the overstory, a continuous homogeneous shrub layer in the middle layer, and a grass layer overlying the soil surface (Kuusk et al., 2014). The forest scene is divided into four parts: the illuminated canopy, the illuminated ground vegetation, the sheltered canopy and the sheltered ground vegetation. The radiances of these elements are estimated based on geometrical and radiative transfer concepts. Tree crown shapes are modeled as rotating ellipsoid or cones in the upper and cylinders in the lower part. Leaves and branches are spherical uniformly distributed in the crown. The two-layer homogeneous canopy reflectance model ACRM by Kuusk (2001) is applied for the calculation of the bidirectional reflectance of ground vegetation (Kuusk and Nilson, 2002). FRT was expected to be suitable for burn severity estimation derived according to the condition of these three vegetation strata. A full list of vegetation parameters used in the FRT model is presented in Table 2. The PROSPECT model (Jacquemoud and Baret, 1990) was coupled into FRT RTM to simulate leaf-level reflectance and transmittance. The valid range and default value of each vegetation parameter were assigned

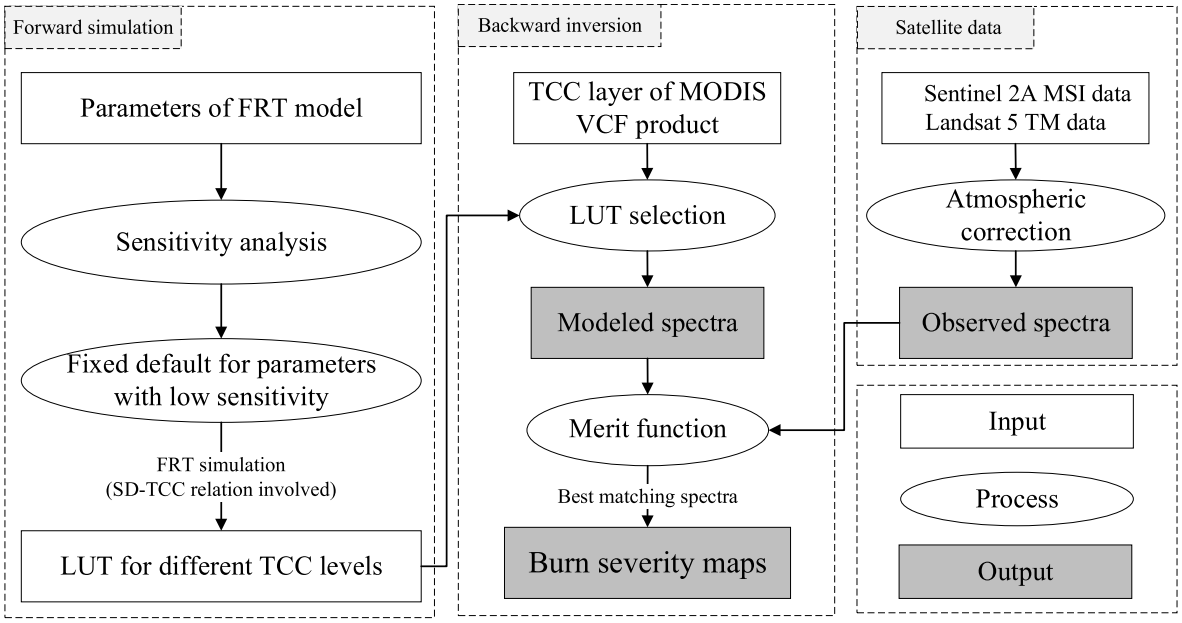

Fig. 4. Methodological flowchart of this study.

based on the FRT user guide (Kuusk and Nilson, 2002).

2.3.2. EFAST sensitivity analysis

Sensitivity analysis is one of the most effective tools to ascertain the key parameters and improve operating efficiencies of an RTM by helping to select the variables that can be fixed and with that decrease the number of simulations in the LUT. In this study, the Extended Fourier Amplitude Sensitivity Test (EFAST) method was used to quantify the importance of the input parameters to the modeled spectra. EFAST sensitivity is robust and efficient for multi-parameter nonlinear complex models (Wang et al., 2013) and has been widely used in hydrological, ecological, and meteorological modeling. It combines the Fourier Amplitude Sensitivity (FAST) algorithm and Sobol algorithm (Nossent et al., 2011). The EFAST sensitivity analysis included sampling and sensitivity index calculation. The main sensitivity index can be obtained using the EFAST analysis method, which reflected the contribution of each input parameter to the model outputs with all test parameters changing simultaneously.

The sensitivity of the FRT model input parameters was represented by the total sensitivity index (TSI) calculated from the EFAST algorithm (Fig. 5). In full spectral bands inversion, each spectral domain from VIS to SWIR contributed to the burn severity estimation. Therefore, the TSI calculation was separated into four parts, VIS (Fig. 5a), NIR (Fig. 5b), SWIR (Fig. 5c), and mean TSI of all spectral bands (Fig. 5d). The input-sensitive parameters were selected in different vegetation layers according to the average TSI for all spectral regions because the CBI was evaluated by considering several vegetation layers. The most sensitive structure parameters of the three vegetation layers (upper story: stand density (*sd*), *BAI/LAI*, crown radius (*cr*); middle story: *LAI2*; and understory: *LAI1*), together with SLW (*SLW3*, *SWL2* and *SLW1*), as the most sensitive biochemical parameter, for each vegetation strata were selected as free variables of the RTM simulation process. In the FRT model, SLW was used to control the biochemical parameters in the PROSPECT model and then determine the leaf color. Finally, the sensitive structure parameters and biochemical parameters of each vegetation strata were selected as the input variables to construct the LUT.

2.3.3. Forward modeling

Parameters of three post-fire vegetation strata (upper tree canopy, middle vegetation layer, and lower vegetation layer) were required to run the FRT model and simulate reflectance for different burn severity classes. According to the sensitivity analysis results, most of the input parameters were insensitive to our selected bands and therefore were fixed to a value using information from remote sensing metadata, previous studies or FRT model defaults (Table 2). The *sd* parameter of the FRT model was used to constrain the TCC variation in this study using the sd-TCC relationship described by Sprintsin et al. (2009). This relationship was derived from a dataset that includes the forest type of our study areas (pine, cypress and eucalyptus) and, therefore, should be valid. The parameter *sd* was set to a range from 0.003 to 0.061, corresponding to TCC from 0% to more than 50% (Sprintsin et al., 2009). Several measurements were used to reduce the errors that may be caused by applying equations from Sprintsin et al. (2009) in our study. Firstly, the *sd* range was divided into six categories (0.003–0.011, 0.013–0.021, 0.023–0.031, 0.033–0.041, 0.043–0.051, and 0.053–0.061) corresponding to six TCC levels (0%–10%, 10%–20%, 20%–30%, 30%–40%, 40%–50%, and higher than 50%) rather than assigning specific values to reduce the corresponding errors between *sd* and TCC. Secondly, the change of *sd* was found to reflect the variation of TCC by checking the field photos of the study sites in the western United States. The *cr* ranged from 0.6 to 4 (Gill et al., 2000), and *BAI/LAI* ranged from 0.3 to 1 (Medhurst and Beadle, 2001). The parameterization of the LAI of the middle and lower vegetation layers was based on the study of O'Grady et al. (2000). *LAI2* was set to a range from 0 to 0.4 while *LAI1* ranged from 0 to 3. For the parameterization of the PROSPECT model to simulate a green and brown leaf, the parameter combination scheme proposed by Kötz et al. (2004) and Lang et al. (2005) was adopted (N = 2.5, C_{ab} = 70 μg/cm^2, C_w = 0.048 g/cm^2 and C_s = 0.2 for green leaf; and N = 2.5, C_{ab} = 20 μg/cm^2, C_w = 0.008 g/cm^2 and C_s = 1.5 for brown leaf). The corresponding relationship between vegetation parameters and CBI is on the basis of the criterion of CBI evaluation. In addition to the post-fire vegetation parameters, the background parameters should also be considered to simulate the post-fire environment. The background short-term after wildfire will be mainly comprised of soil and charcoal. Therefore, three reference spectra for the background layer were considered for the model input: soil, dark charcoal (DCH) and light charcoal (LCH, a mixture of charcoal and ash) (Fig. 6). The soil spectrum was measured from a medium-moisture sandy soil, while both dark and light charcoal spectra were measured with a GER 2600 field spectro-radiometer (Geophysical & Environmental Research Corporation, Millbrook, NY) by De Santis et al. (2009).

Table 2
The input vegetation parameters and default range used for the parameterization of the FTR RTM.

Parameters	Units	Symbol	Range	Defaults
*** Upper tree canopy ***				
stand density	m^2	*sd*	0.001–0.08	0.1115
tree height	m	*th*	10–30	15.9
crown length	m	*cl*	5–10	4.2
cylinder	m	*cy*	0–10	0
crown radius	m	*cr*	0.2–5	1.5
DBH	cm	*DBH*	2–25	18
total dry leaf weight	kg/tree	*m*	1.1–3	2.67
leaf weight per area	g/m^2	*SLW3*	30–180	160
eccentricity parameter of LAD		*eln3*	0–4.5	3.99
modal leaf angle	(°)	*thm3*	0–90	53.57
shoot length	m	*sl*	0.05–0.6	0.1
BAI/LAI ratio		*BAI/LAI*	0.01–1	0.3123
grouping index		*GI*	0.6–2.8	1.69
H-G asymmetry		*HG*	0.1–0.6	0.4
Prospect 3				
water content	% of SLW	*c1*	50–320	240
chlorophyll content	% of SLW	*c2*	0.3–1	0.554
dry matter	% of SLW	*c3*	94–99.9	97.11
leaf str. param.		*N3*	1.6–2.8	1.6016
refraction index ratio		*rir*	0.6–1.2	0.9
*** **Middle vegetation layer** ***				
LAI2_ground		*LAI2*	0.01–6	0.208
HS-parameter		*sl2*	0.02–0.4	0.15
foliage clumping parameter		*clmp2*	0.4–1	1.0
displacement parameter		*szz*	0–2	1.2
eccentricity parameter of LAD		*eln2*	0–4.5	3.99
modal leaf angle	(°)	*thm2*	0–90	53.37
n_ratio2		*n_ratio2*	0.6–1.3	0.991
leaf weight per area	g/m^2	*SLW2*	30–180	81.7
Prospect 2				
water content	% of SLW	*c11*	130–320	139
chlorophyll content	% of SLW	*c21*	0.3–0.8	0.36
dry matter content	% of SLW	*c31*	94–99.8	99.52
brown pigment content	% of SLW	*c41*	0.0002–4	0.1
leaf str. param.		*N2*	1–2.8	1.315
*** **Lower vegetation layer** ***				
LAI1_ground		*LAI1*	0.01–1.1	1.064
HS-parameter		*sl1*	0.02–0.4	0.15
foliage clumping parameter		*clmp1*	0.4–1	1
eccentricity parameter of LAD		*eln1*	0–4.5	3
modal leaf angle	(°)	*thm1*	0–90	75.469
n_ratio1		*n_ratio1*	0.6–1.3	1.224
leaf weight per area	g/m^2	*SLW1*	30–180	78.54
Prospect 1				
water content	% of SLW	*c111*	130–320	134.24
chlorophyll content	% of SLW	*c211*	0.3–0.8	0.425
anthocyanins	% of SLW	*c311*	0.3–0.8	0.733
dry matter content	% of SLW	*c411*	94–99.8	98.343
leaf str. param.		*N1*	1–2.5	1.0053

Considering the potential ill-posed problem caused by unrealistic combinations of input variables, a supervised simulation scheme was used to alleviate the error, as it performs better than full-range variations (Chuvieco et al., 2007; De Santis et al., 2009). The background was considered as comprised by charcoal and soil. The same range of simulation scheme was adopted for the upper canopy parameters of the sites in northern Australia and the western United States to validate the universality of the RTM method on estimating burn severity. However, different simulation scenarios were developed in the middle and understory layers because field surveys at the study sites in the western United States were undertaken one-year post-fire while in northern Australia they were undertaken immediately after the fire. The different simulation scheme of middle and understory layers was used to represent the different recovery patterns of the vegetation in the middle and lower layers. The simulated CBI ranges from 0.5 to 3 with a step of 0.1. An example of the combination of input parameters used for LUT generation is listed in Table 3. The field survey for the western United States (one-year post-fire) showed no observable LCH on the soil surface from the field photos. Therefore, we did not undertake an LCH scenario simulation in western United States study sites. There were a total of 960 and 780 combinations of input parameters used to construct the LUTs for northern Australia and the western United States, respectively.

2.3.4. RTM model inversion

A LUT algorithm was used as the inversion method in this study to retrieve burn severity from Landsat-5 and Sentinel-2A data. A Spectral Angle Mapper (SAM) classification algorithm was used as the merit function to find the simulated spectral reflectance spectrum that best matched the observed spectrum. SAM is a pixel-based supervised classification technique that solves spectral similarity by calculating the spectral angle (SA) between two spectral vectors (Dennison et al., 2004; Kruse et al., 1993). This angle is independent of the length of vectors, so it is insensitive to illumination or albedo effects. Therefore, SAM can eliminate most of the errors caused by topographic fluctuations (De Santis and Chuvieco, 2007). In the backward inversion, the minimum SA between simulated and satellite-derived spectral reflectance was used to estimate the structure and biochemical variables of the vegetation that determined a certain CBI value. The backward inversion was conducted using all Landsat-5 TM reflective spectral bands and nine Sentinel-2A MSI bands and FRT RTM with (RTM + TCC) and without (RTM + GOS) TCC constraint. In the inversion process of RTM + GOS, the estimated CBI is the result of global optimal search after matching the observed spectra with all simulated spectra. In addition to the mentioned spectral bands of Landsat-5 and Sentinel-2A, the post-fire NBR was also included as an extra vector to improve the estimates of RTM model inversion. Model inversion was carried out in the LUT corresponding to the specific TCC level according to the input MODIS VCF data. Given that the significance and utility of using Sentinel 2A MSI VRE bands to estimate burn severity has not been previously evaluated, we also evaluated the role of the VRE bands in RTM inversion by comparing the accuracy between the burn severity estimation results with and without VRE bands.

2.4. Accuracy assessment

Burn severity was assessed against field data collected in northern Australia and the western United States as burn severity classes and CBI values, respectively. The accuracy of the method proposed in this study was evaluated using the confusion matrix in northern Australia, while linear correlation and root mean square error (RMSE) between field measured and estimated burn severity was used in the western United States. The results derived from our method were compared to those obtained using two standard empirical spectral indices broadly used to map burn severity, dNBR and RdNBR.The empirical methods were used as a point of reference, as empirical models are still broadly used in fire management for mapping fire severity. A threshold with less manual interference is needed for the binary classification using an empirical method. In this study, the threshold calculation method based on dNBR and RdNBR proposed by Edwards et al. (2018) was adopted in the northern Australian study area (Eq. (1)).

$$\mathrm{Ths} = (((\mu_1 - \sigma_1) - (\mu_2 - \sigma_2))/2) + (\mu_2 - \sigma_2) \quad (1)$$

where μ_1 and σ_1 represent the *mean* and *standard deviation* of the field-measured SV class, and μ_2 and σ_2 represent the *mean* and *standard deviation* of the field-measured NSV class, respectively.

A second-order polynomial function was used to construct the empirical model by fitting field-measured CBI with both dNBR and RdNBR in the study sites of the western United States following previous studies (De Santis et al., 2010; Soverel et al., 2010). The dNBR and RdNBR images of fires in the western United States were also provided by the MTBS. The latest scene with good quality before a fire was selected as the pre-fire image to derive dNBR and RdNBR.

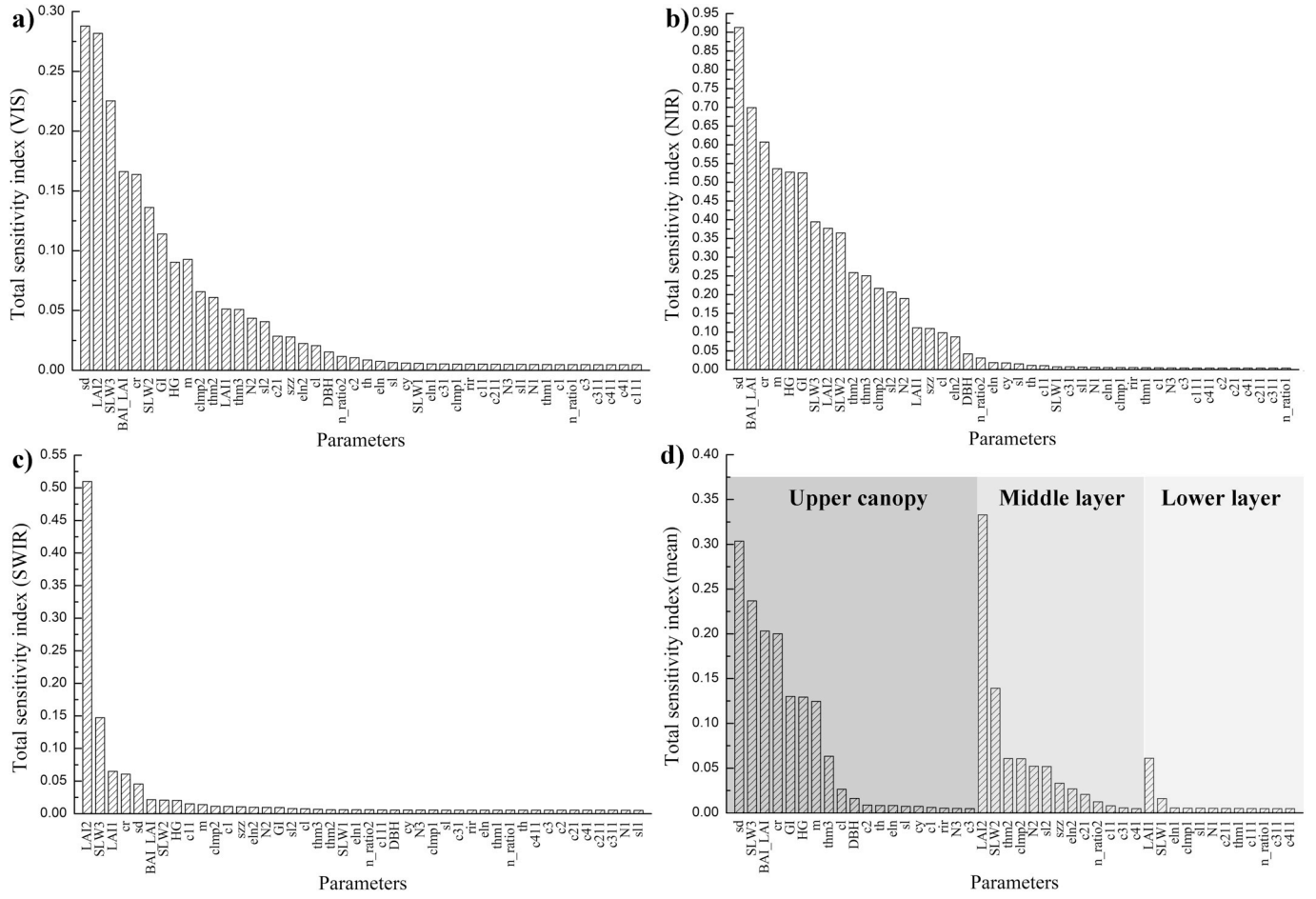

Fig. 5. Total sensitivity index (TSI) of (a) visible bands (VIS), (b) the near-infrared band (NIR), (c) shortwave infrared bands (SWIR) and (d) the mean TSI of the FRT model variables in each vegetation strata.

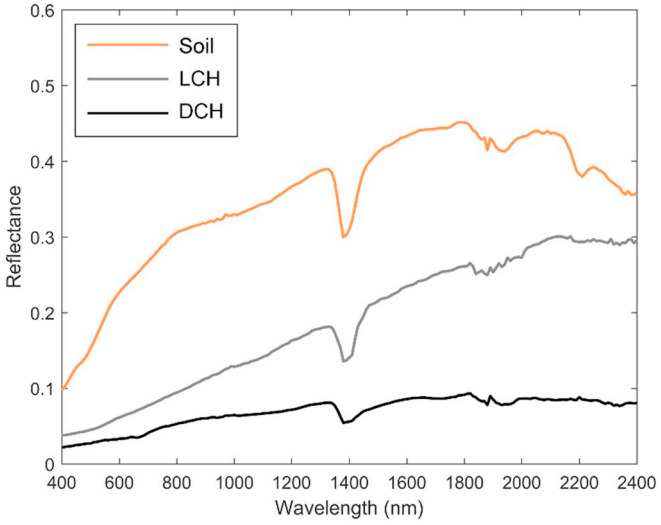

Fig. 6. Reference spectra used as post-fire background; soil, dark charcoal (DCH) and light charcoal (LCH, a mixture of charcoal and ash). The reference spectra were provided by De Santis et al. (2009).

3. Results

3.1. Validation in northern Australia

3.1.1. Influence of TCC on the spectral response of burnt plots

The surface reflectance and post-fire NBR of the field plots were extracted from Sentinel 2A MSI and averaged by fire severity level (SV and NSV) and TCC (< 5%, 5%–10%, 10%–20% and > 20%) to demonstrate the influence of TCC on the spectral response and confusion between burn severity levels (Fig. 7). The SA was used to quantitatively evaluate the similarity of different spectra. Fig. 7a1 and 7b1 represent the extracted mean reflectance from all field plots without constraining TCC. The average reflectance of all field plots masked the reflectance variation between different TCC levels. By classifying the field plots according to TCC, the difference of SA under different TCC levels is widened. The SA between the spectra extracted from the plots with NSV burn severity, TCC of < 5% and > 20% (Fig. 7a2 and 7a5) was 0.61 and 0.1 for SV plots (Fig. 7b2 and 7b5), demonstrating that the spectra of NSV plots (Fig. 7a) were more susceptible to TCC than the spectra of SV plots (Fig. 7b). The SA between NSV plots when TCC is < 5% (Fig. 7a2) and SV plots when TCC is 10%–20% (Fig. 7b4) is 0.13, smaller than the SA between NSV and SV plots within the same TCC range of 10%–20% (Fig. 7a4 and 7b4, 0.32). In the model inversion process, smaller SA means higher spectral similarity and thus a more similar burn severity. If TCC is not constrained in the model simulation and inversion process, there will be a severe overestimation for NSV burn severity level in low TCC regions. The spectral analysis results of the field plots are consistent with our theoretical analysis in Fig. 1, that

Table 3
Combination of input parameters used as inputs in the FRT model for the simulation of reflectance corresponding to different CBI values. The stand density (varied from 0.003 to 0.061 with a step of 0.002) was used to constrain TCC in the model simulation. The cells for northern Australia (AUS) and western United States (US) represent the combined middle and lower vegetation parameters in AUS and US, respectively. DCH = dark charcoal; LCH = light charcoal; NAN = non-vegetation.

	CBI	0.5	1	1.5	1.8	2	2.3	2.5	2.8	3
AUS	stand density	0.003–0.061								
	crown radius	4	3	2.5	2.2	1.9	1.6	1.2	0.8	0.6
	BAI/LAI	0.3	0.38	0.48	0.54	0.58	0.68	0.72	0.84	1
	leaf color	Green	Green	Green	Green	Green	Green	Green	Brown	Brown
	LAI2	0.5	0.4	0.3	0.15	0.1	0.05	0.05	NAN	NAN
	leaf color	Green	Brown	Brown	Brown	Brown	Brown	Brown	NAN	NAN
	LAI1	3	0.3	NAN	NAN	NAN	NAN	NAN	NAN	NAN
	leaf color	Brown	Brown	NAN	NAN	NAN	NAN	NAN	NAN	NAN
	sub-stratum	0.6soil + 0.4DCH	0.5soil + 0.5DCH	DCH	DCH	DCH	DCH	DCH/LCH	DCH/LCH	DCH/LCH
US	LAI2	0.5	0.1	NAN	NAN	NAN	NAN	NAN	NAN	NAN
	leaf color	Brown	Brown	NAN	NAN	NAN	NAN	NAN	NAN	NAN
	LAI1	3	2	1	0.4	0.1	0.1	0.1	NAN	NAN
	leaf color	Green	Green	Green	Green	Green	Green	Green	NAN	NAN
	sub-stratum	0.8soil + 0.2DCH	0.8soil + 0.2DCH	0.7soil + 0.3DCH	0.6soil + 0.4DCH	0.5soil + 0.5DCH	0.4soil + 0.6DCH	0.3soil + 0.7DCH	0.1soil + 0.9DCH	DCH

the same burn severity will correspond to different spectral signatures and the same spectral signature could correspond to different levels of burn severity with the variation of TCC.

Two sample spectrums within different burn severity levels simulated by FRT RTM were also extracted (Fig. 8). Fig. 8a and b shows the simulated spectra of NSV and SV burn severity levels within different TCC levels, respectively. It can be seen from Fig. 8 that FRT RTM has the capacity to simulate the canopy reflectance with different TCC levels, and the multi-bands can provide more spectral information to identify different burn severity levels. The characteristics of the spectrum simulated by FRT RTM are in agreement with the analysis results of the field plots. The same burn severity showed different characteristics with the variation of TCC, and the spectra of the NSV burnt level were more susceptible to TCC than spectra of the SV burnt level. Therefore, model inversion carried out in the LUT corresponding to the specific TCC level can significantly reduce the overestimation errors in low TCC regions for the NSV burnt level. However, the reflectance of the plots with TCC < 10% was mainly dominated by charcoal and dead litter, whilst vegetation had much less influence. This resulted in ubiquitous spectral confusion between NSV and SV (Fig. 7a2, 6a3, 6b2, and 6b3) with the SA with the same TCC (around 0.22), indicating that spectral confusion with low TCC can't be avoided completely.

3.1.2. Evaluation of burn severity estimates

Burn severity was estimated using the FRT RTM + GOS and FRT RTM + TCC methods. The producer's accuracy of the RTM + GOS at study site 1 was 93% and 38% for the SV and NSV burn severity levels, respectively (Table 4). While most of the plots classified as SV were correctly classified, overestimation occurred for the NSV plots. The use of TCC information to invert FRT RTM (RTM + TCC) improved the producer's accuracy from 38% to 85% for NSV at the cost of a decrease of the producer's accuracy of SV from 93% to 73%. The user's accuracy of SV increased from 50% to 76% while it decreased from 90% to 82% for NSV. The overall classification accuracy improved from 60% to 80%, and the kappa coefficient increased from 0.27 to 0.58 when integrating TCC information in RTM parameterization and backward inversion (Table 4). Model performances were similar for study site 2. The producer's accuracy of the NSV increased from 72% to 83%, the user's accuracy of the SV improved from 22% to 32% and the overall accuracy, and the kappa coefficient increased from 73% to 83% and 0.25 to 0.38, respectively (Table 4). Merging the results for both sites demonstrated that the estimation accuracy significantly improved by use of the RTM + TCC method (Table 4). The overall accuracy and kappa coefficient improved from 65% to 81%, and 0.35 to 0.55, respectively. These improvements demonstrated that restricting the TCC in the inversion process is a valid approach for both the LDS (site 1) and EDS (site 2) fires.

For comparison, burn severity was also obtained using two standard spectral indices broadly used to map burn severity, dNBR and RdNBR (Table 4). For site 1, the producer's accuracy of NSV reached 96% and 99% for dNBR and RdNBR, respectively but the accuracy for SV was very low (26% and 6% for dNBR and RdNBR, respectively). The overall accuracy, 68% for dNBR and 62% for RdNBR, and kappa coefficient, 0.25 for dNBR and 0.06 for RdNBR, were also unacceptable. These poor results were due to the fact that the threshold used for the binary burn severity classification was too high and led to misclassification of most of the SV plots as NSV, indicated that this automatic threshold selection method is unstable and have no universality. For study site 2, the overall accuracy was higher (85% for dNBR, 84% for RdNBR) and similar to the overall accuracy of the RTM + TCC method (83%). The empirical methods produced slightly lower kappa coefficient, 0.3 and 0.31 for dNBR and RdNBR, respectively, than the RTM + TCC method (0.38). Similar to study site 1, the burn severity of site 2 field SV plots was highly underestimated based on dNBR and RdNBR (producer's accuracy of SV, 50% and 56% for dNBR and RdNBR, respectively). However, due to the marked difference in the number of SV (16 plots)

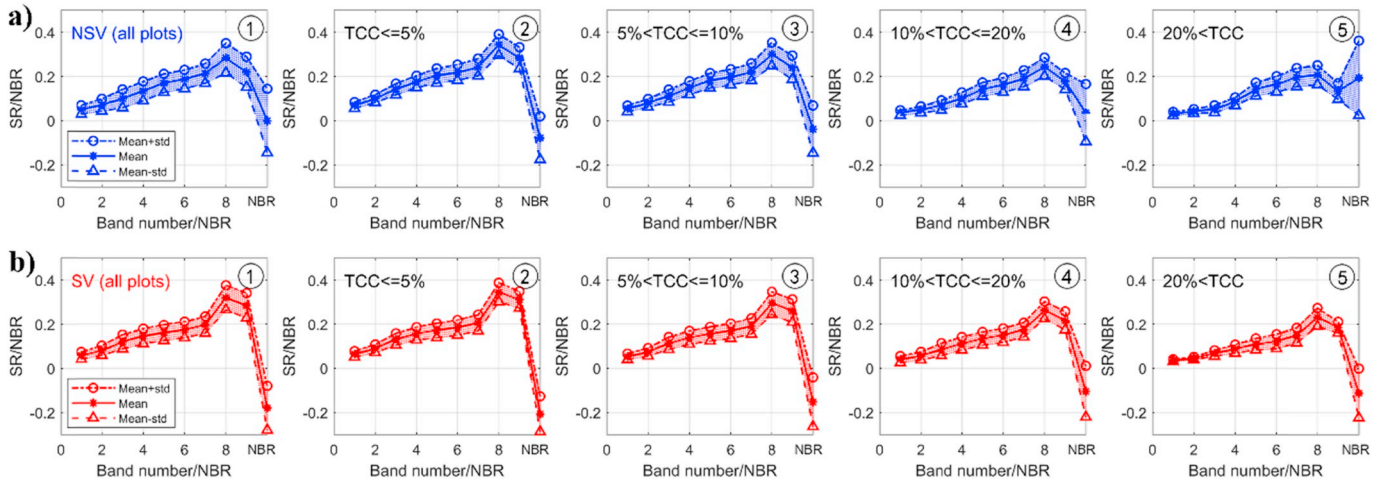

Fig. 7. Mean and standard deviations (std) of the Sentinel-2A MSI spectral signatures of plots with (a) *not severe* (NSV) and (b) *severe* (SV) burn severity and different tree canopy cover (TCC) values at northern Australian study sites. The x-axis represents the nine spectral bands and post-fire NBR, the y-axis represents the value of the reflectance (SR) and post-fire NBR. The first column represents the reflectance from all field plots without constraining TCC; other columns represent different TCC levels.

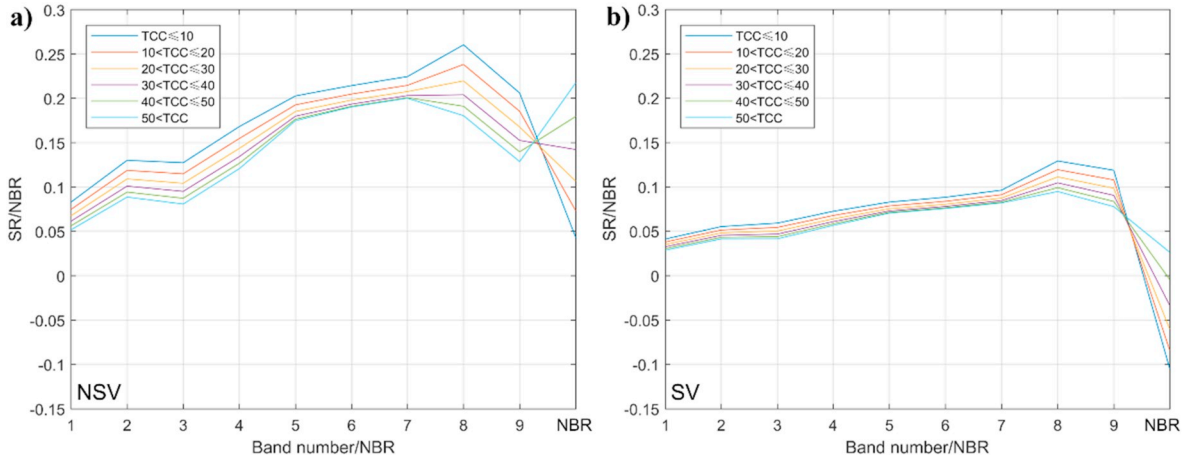

Fig. 8. Two sample spectrums within different TCC levels simulated by FRT RTM in (a) NSV and (b) SV burn severity levels. In order to make a more intuitive comparison with the spectral response of the field plots, only the reflectance (SR) and NBR of these corresponding bands were selected.

and NSV (163 plots) plots, the high producer's and user's accuracies of NSV largely enhanced the overall accuracy. When merging the results from both sites, the overall accuracy using empirical methods (74% and 70% for dNBR and RdNBR, respectively) was higher than the RTM + GOS method (65%) and lower than the RTM + TCC method (81%). However, the SV producer's accuracy and overall kappa coefficient based on dNBR (28%, 0.25) and RdNBR (12%, 0.06) were unacceptable. Overall, the RTM + TCC method showed the best performance (overall accuracy: 81%, kappa coefficient: 0.55).

To clarify the role of VRE bands in the retrieval of burn severity using Sentinel-2A MSI and RTM inversion, we compared the results of inverting FRT RTM + TCC with and without the VRE bands. For study site 1, the overall accuracy and kappa coefficient without using VRE bands were 80% and 0.58, respectively (Table 4). The producer's and user's accuracies for the SV and NSV are only slightly different to the results using VRE bands. For study site 2, the accuracy was the same, independent of the VRE bands. This indicated that the inclusion of the VRE bands of Sentinel-2A MSI did not significantly affect the burn severity estimation compared to using full spectral bands and the inversion of RTM. This was probably because other spectral bands, or post-fire NBR, mask the sensitivity of the VRE bands to fire. The focus of this study is burn severity estimation, so the dNBR as well as visual interpretation were used to extract burn area. Burn severity maps for the two study sites of northern Australia were produced based on the burn area extraction and RTM + TCC method (Fig. 9). Fires in site 1 represented LDS fires, more severe than the patchy EDS fires of study site 2.

3.2. Validation in the western United States

3.2.1. Influence of TCC on the spectral response of burnt plots

The surface reflectance and post-fire NBR of the field plots in the western United Sates were extracted from Landsat-5 TM and averaged by fire severity level and TCC (< 10%, 10%–20%, 20%–50% and > 50%) to demonstrate the influence of TCC on the spectral response and confusion between burn severity levels (Fig. 10). In this case, the burn severity was classified into low, moderate and high using CBI threshold values of 2 and 2.5. Similar to the NSV results in northern Australia (Fig. 7a), the spectral response of the low and moderate burnt levels (Fig. 10a and b) showed obvious differences between different TCC, demonstrating that the low and moderate burnt levels are more susceptible to TCC. The spectra of the high burn severity level were less affected by TCC variability (Fig. 10c). This was also observed from the SA between the spectra of lowest and highest TCC within the same burn severity. The SA was 1.27 (Fig. 10a1 and 10a5), 0.98 (Fig. 10b1 and 10b5) and 0.08 (Fig. 10c1 and 10c5) for low, moderate and high burn severity, respectively. When the TCC exceeded 50%, the spectrum of

Table 4
Confusion matrix comparing burn severity observed in the field and estimated at study sites 1 and 2, and the two study sites together. RTM + GOS represents the method based on FRT RTM and global optimal search (without constraining TCC). RTM + TCC represents the method that considered the variation of TCC in model simulation and all reflective bands were used in backward inversion. RTM + TCC (without VRE bands) represents the method that considered the variation of TCC in model simulation and reflective bands other than red edge bands are considered in backward inversion. dNBR and RdNBR are standard empirical spectral indices broadly used to map burn severity. The NSV and SV in this table represent the *not-severe* and *severe* burn severity levels.

			RTM + GOS				RTM + TCC				dNBR				RdNBR				RTM + TCC (without VRE bands)			
			NSV	SV	Totals	Producer's accuracy	NSV	SV	Totals	Producer's accuracy	NSV	SV	Totals	Producer's accuracy	NSV	SV	Totals	Producer's accuracy	NSV	SV	Totals	Producer's accuracy
Study site 1	Field data	NSV	**69**	113	182	38%	**154**	28	182	85%	**175**	7	182	96%	**180**	2	182	99%	**157**	25	182	86%
		SV	8	**113**	121	93%	33	**88**	121	73%	90	**31**	121	26%	114	**7**	121	6%	35	**86**	121	71%
		Totals	77	226	**303**		187	116	**303**		66	38	**303**		294	9	**303**		192	111	**303**	
		User's accuracy	90%	50%		**60%**	82%	76%		**80%**	94%	82%		**68%**	61%	78%		**62%**	82%	77%		**80%**
	Kappa		**0.27**				**0.58**				**0.25**				**0.06**				**0.58**			
Study site 2	Field data	NSV	**118**	45	163	72%	**135**	28	163	83%	**145**	18	163	89%	**142**	21	163	87%	**135**	28	163	83%
		SV	3	**13**	16	81%	3	**13**	16	81%	8	**8**	16	50%	7	**9**	16	56%	3	**13**	16	81%
		Totals	121	58	**179**		138	41	**179**		153	26	**179**		149	30	**179**		138	41	**179**	
		User's accuracy	98%	22%		**73%**	98%	32%		**83%**	95%	31%		**85%**	95%	30%		**84%**	98%	32%		**83%**
	Kappa		**0.25**				**0.38**				**0.30**				**0.31**							
Two study sites	Field data	NSV	**187**	158	345	54%	**289**	56	345	84%	**320**	25	345	93%	**322**	23	345	93%	**292**	53	345	85%
		SV	11	**126**	137	92%	36	**101**	137	74%	98	**39**	137	28%	121	**16**	137	12%	38	**99**	137	72%
		Totals	198	284	**482**		325	157	**482**		418	64	**482**		443	39	**482**		330	152	**482**	
		User's accuracy	94%	44%		**65%**	89%	64%		**81%**	77%	61%		**74%**	73%	41%		**70%**	88%	65%		**81%**
	Kappa		**0.35**				**0.55**				**0.25**				**0.06**				**0.55**			

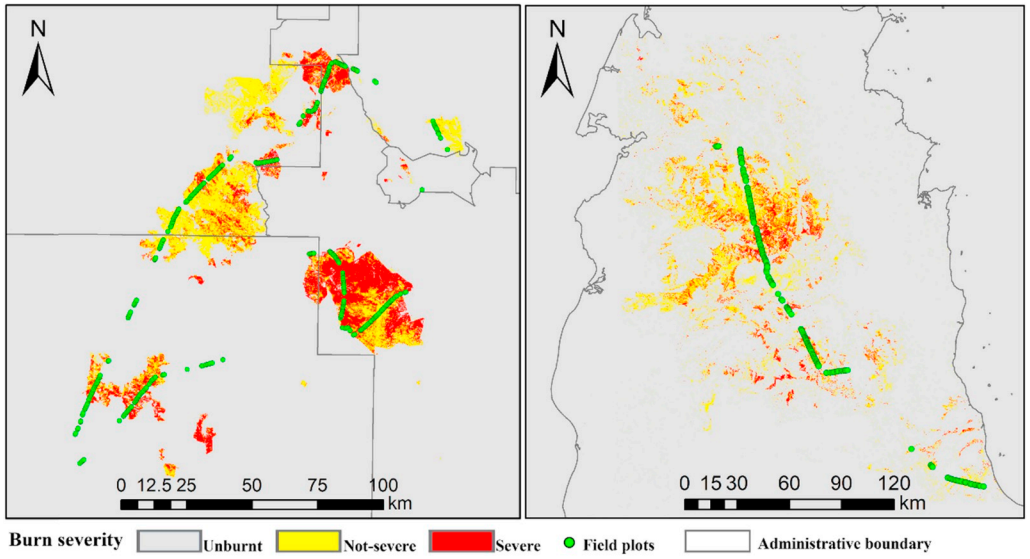

Fig. 9. Burn severity maps for study sites 1 (left) and 2 (right) of northern Australia obtained using the RTM + TCC method developed in this study.

the high burnt levels showed similar characteristics to the moderate and low burnt levels with the lower TCC. More specifically, high burn severity with TCC > 50% (Fig. 10c5) demonstrated spectral confusion with moderate burn severity when TCC was 20%–50% (Fig. 9c5 and 9b4, SA = 0.13) and moderate burn severity when TCC was 20%–50% demonstrated spectral confusion with low burn severity when TCC was 10%–20% (Fig. 10b4 and 10a3, SA = 0.19). The SA between high and moderate burn severity when TCC is > 50% (Fig. 10c5 and 10b5, SA = 0.39) and the SA between moderate and low burn severity when TCC is 20%–50% (Fig. 10b4 and 10a4, SA = 1.13) was higher than the corresponding cross burn severity SA. Consequently, the low burn severity plots were expected to be overestimated at low TCC and the moderate to high burn severity is expected to be underestimated when TCC was not considered for the retrieval of fire severity.

Three sample spectrums within different TCC and different burn severity levels simulated by FRT RTM were also extracted (Fig. 11). Fig. 11a, b and 10c show the simulated spectrum of low, moderate, and high burn severity within different TCC levels, respectively. Fig. 11 shows that FRT RTM can simulate burn severity levels in different TCC levels. The same burn severity showed different characteristics with the variation of TCC, and the spectra of low and moderate burnt level were more susceptible to TCC than the high burnt level. Consistent with the spectral analysis results of field plots, model inversion carried out in the LUT corresponding to the specific TCC level according to the input

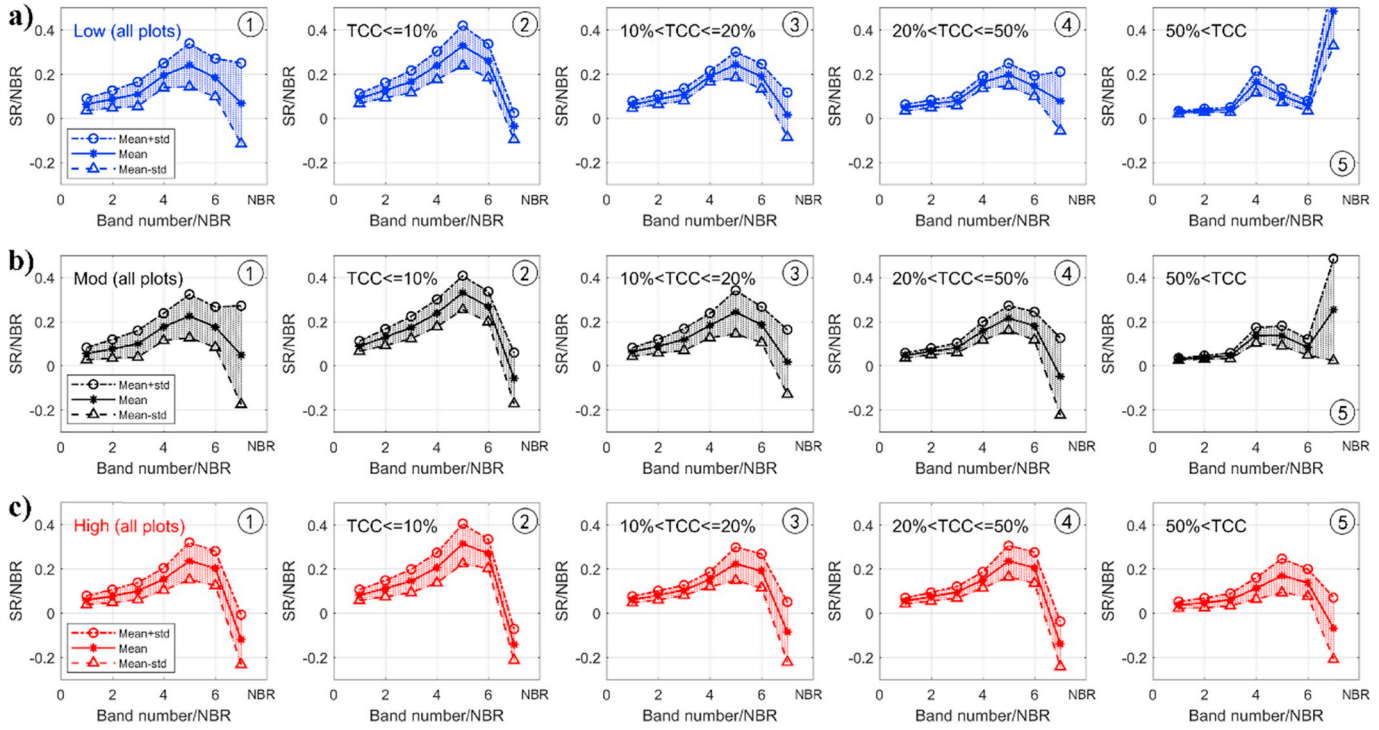

Fig. 10. Mean and standard deviations (std) of the Landsat-5 TM spectral signatures of plots with (a) low, (b) moderate and (c) high burn severities and TCC ranges in the western United States study sites. The x-axis represents the six spectral bands and post-fire NBR, and the y-axis represents the spectral reflectance (SR) and post-fire NBR.

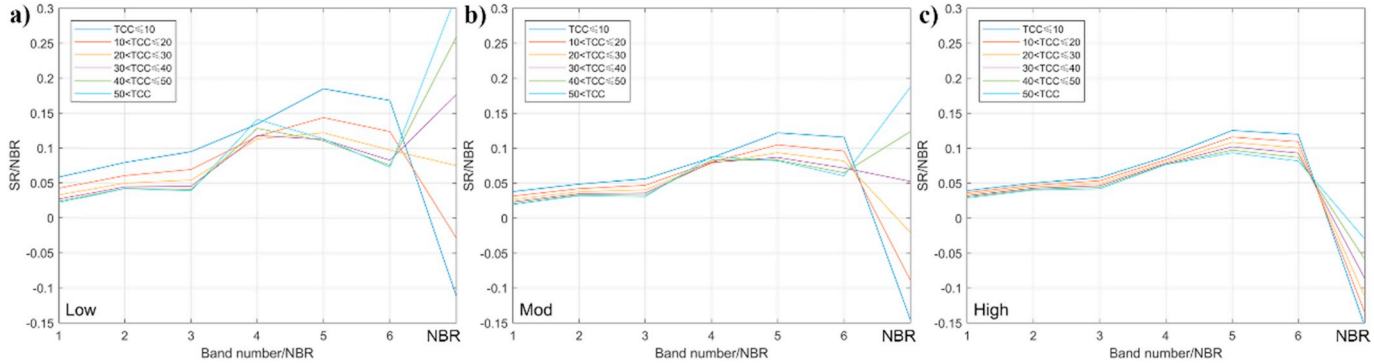

Fig. 11. Three sample spectrums within different TCC levels simulated by FRT RTM in (a) low, (b) moderate and (c) high burn severity levels. In order to make a more intuitive comparison with the spectral response of the field plots, only the reflectance (SR) and NBR of these corresponding bands were selected.

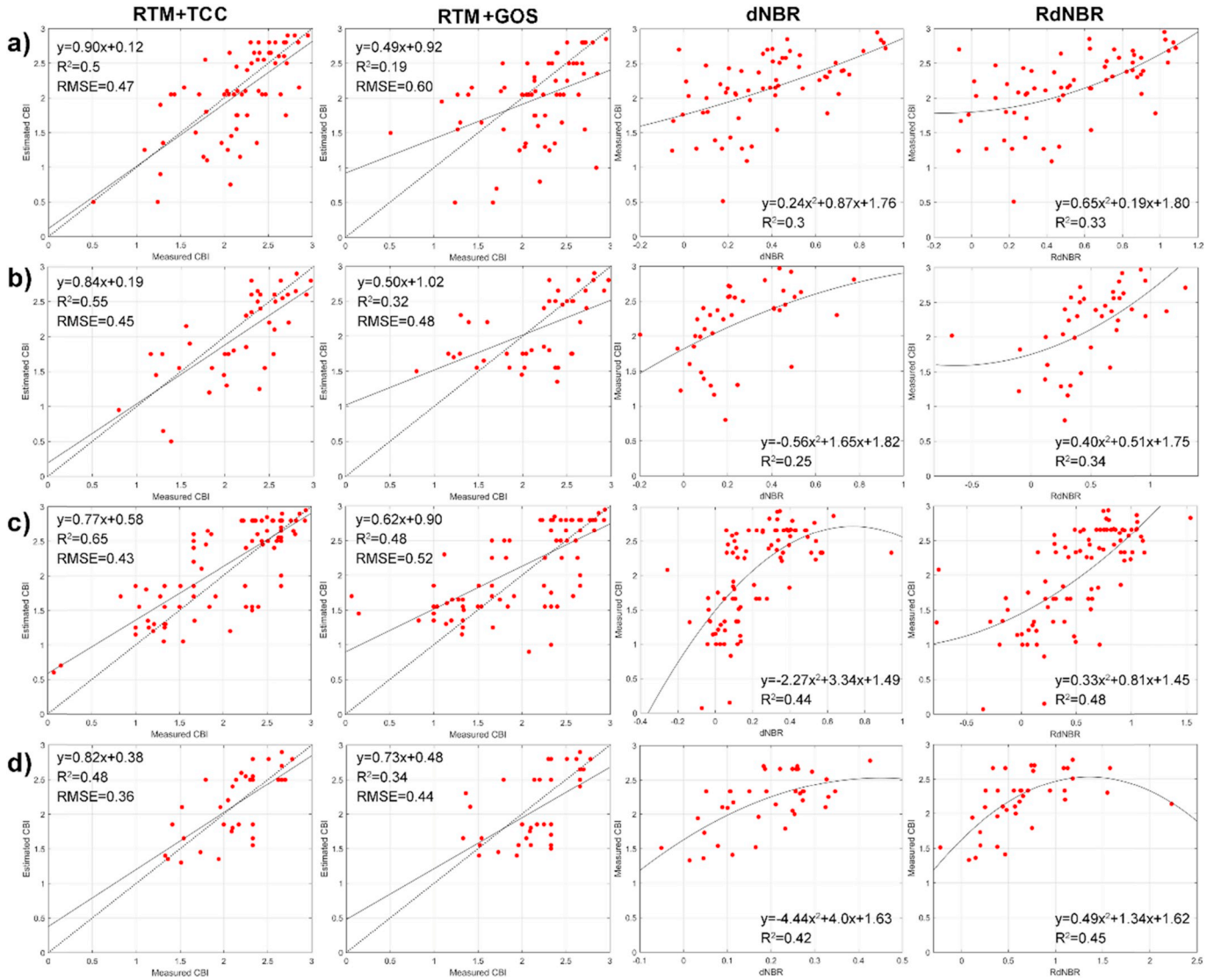

Fig. 12. Field-observed versus estimated burn severity (expressed as CBI) for (a) study site 3, (b) study site 4, (c) study site 5 and (d) study site 6 of the western United States. The dashed line represents the 1:1 line, the solid line is the fitted line. From left to right, each column represents the estimation results based on the RTM + TCC method, the RTM + GOS method, dNBR, and RdNBR, respectively.

MODIS VCF data can significantly reduce the overestimation errors in low TCC regions for low burn severity and the underestimation errors in high TCC regions for high burn severity.

3.3. Evaluation of burn severity estimates

The CBI was estimated based on RTM + TCC, RTM + GOS, dNBR, and RdNBR at the four study sites of the western United States (Fig. 12). Some field plots with low burn severity (CBI < 2) were overestimated.

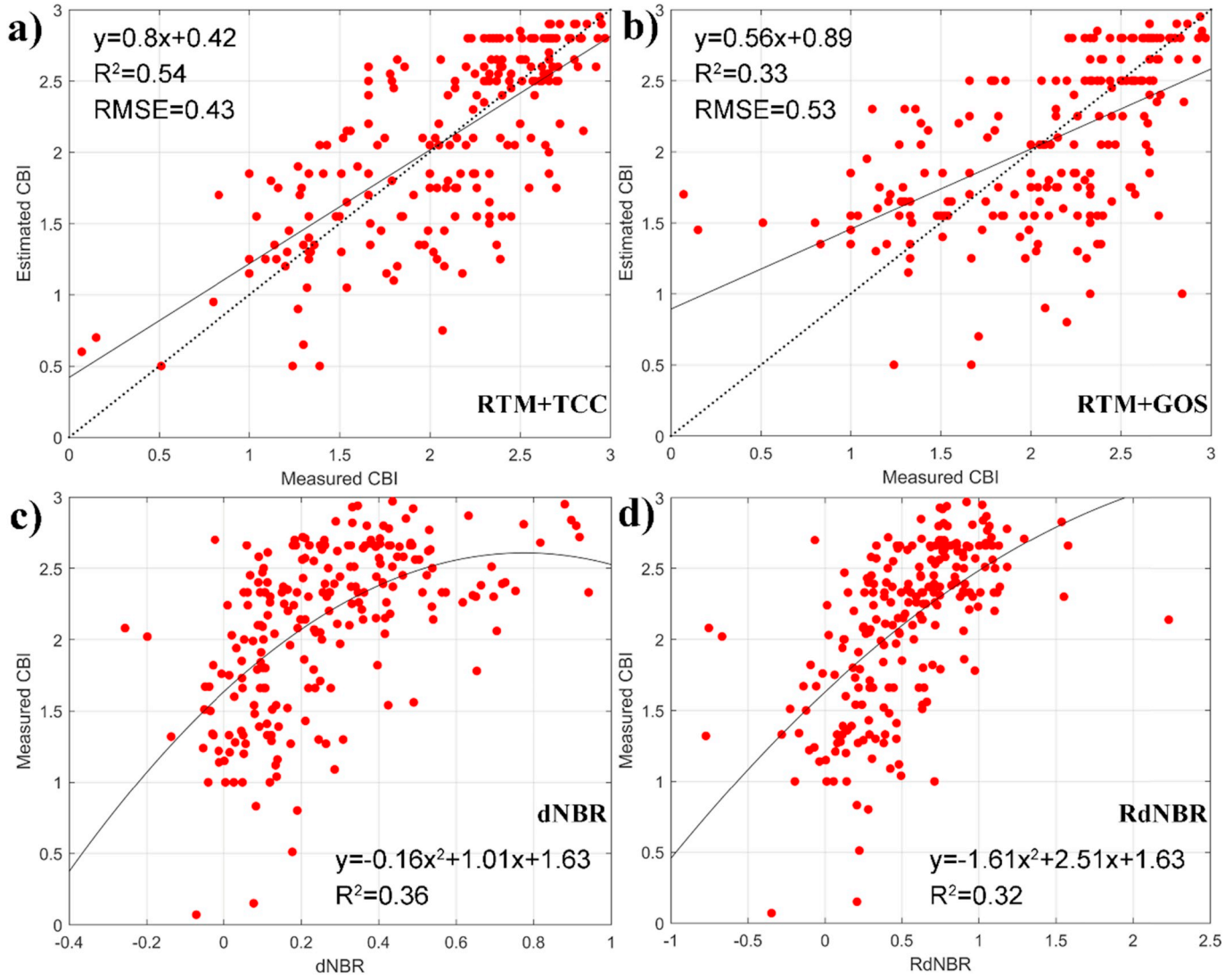

Fig. 13. Field-observed and estimated burn severity (expressed as CBI) for all field plots. Estimated results based on (a) the RTM + TCC method, (b) the RTM + GOS method, (c) dNBR, and (d) RdNBR.

Conversely, some of the plots with moderate ($2 \leq$ CBI < 2.5) and high (CBI ≥ 2.5) burn severity were underestimated when estimating burn severity using the RTM + GOS method (second column in Fig. 12). The RTM + TCC method reduced the underestimation and overestimation errors, significantly improved the determination coefficients (R^2) (from 0.19 to 0.5, from 0.32 to 0.55, from 0.48 to 0.65, from 0.34 to 0.48 for study sites 3 to 6, respectively) and decreased the RMSE (from 0.6 to 0.47, from 0.48 to 0.45, from 0.52 to 0.43, from 0.44 to 0.36 for study sites 3 to 6, respectively). This reduction in error was also observed in the slope fitting in each study site of the RTM + GOS method (0.49 for study site 3, 0.50 for study site 4, 0.62 for study site 5, and 0.73 for study site 6). By integrating TCC into the parameterization and inversion of FRT RTM, the slope of the regression between the observed and estimated CBI at each study site increased to 0.9, 0.84, 0.77, and 0.82, for sites 3 to 6, respectively. Among these four study sites, study site 3 presented the highest TCC level and led to the most severe underestimation of moderate to high burn severity when using the RTM + GOS method. The most severe overestimation occurred when CBI was lower than 1.5 in study sites 4 and 5. By contrast, the performance of the empirical models using dNBR and RdNBR was much less stable among these four study sites (Fig. 12) than that of the RTM + TCC method. The fitted empirical model between field-measured CBI and the two spectral indices varied considerably between study sites while the RTM + TCC method was more stable.

When all field plots from the four study sites were merged, the R^2 improved from 0.33 to 0.54, the RMSE decreased from 0.53 to 0.43, and the fitted slope increased from 0.56 to 0.8, when including information of TCC in the RTM, in comparison to the RTM + GOS (Fig. 13a and b). The R^2 values between CBI observed and estimated using dNBR (Fig. 13c) and RdNBR (Fig. 13d) were similar to that between CBI observed and estimated using the RTM + GOS method (0.33) but lower than using the RTM + TCC method (0.54).

In addition to the burn severity data measured in the field, field photos at each location are included as a reference of the field conditions related to the CBI assessments (Fig. 14). There is a general overestimation for low burn severity in low tree-covered regions (Fig. 14a–c). The field CBI of three plots with low TCC value ($< 18\%$) were 1.33, 0.15 and 1.12 (Fig. 14a–c). CBI estimates, based on the RTM + GOS method, overestimated the CBI (2.25, 1.45, and 2.3, respectively). By integrating TCC in the parameterization and inversion of FRT RTM, the overestimation errors were reduced, obtaining CBI values of 1.4, 0.7, and 1.7, respectively, which are closer to the observations. For regions with dense TCC (Fig. 14d–f), the spectrum of high and moderate burn severity was similar to the moderate and low burn severity in the lower TCC region (Fig. 10c5, 9b4, and 9a3, respectively). The observed CBIs were 2.38, 2.2 and 2.84 while the CBI estimates,

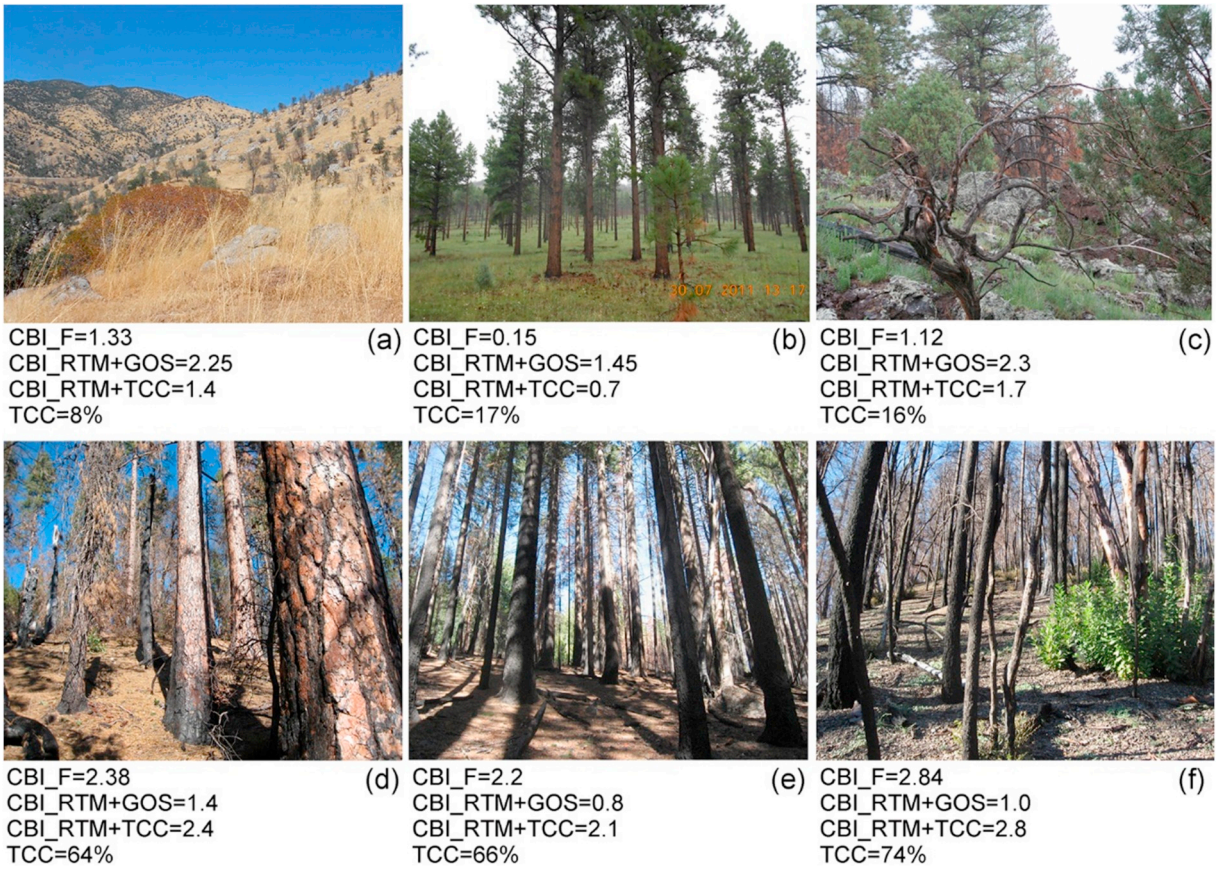

Fig. 14. Examples of field photos to demonstrate the validity of the method proposed in this study to correct overestimation and underestimation errors in retrieving CBI using the RTM + TCC method. CBI_F, CBI_RTM + GOS, and CBI_RTM + TCC represent the CBI values of field measurements and based on the RTM + GOS, and RTM + TCC methods, respectively. TCC represents the percent tree canopy cover at the field plots.

using the RTM + GOS method, gave values of 1.4, 0.8 and 1.0, respectively. The RTM + TCC method corrected the underestimation errors produced by the spectral confusions and obtained CBI values of 2.4, 2.1 and 2.8, respectively. Burn severity maps for the 15 fires that occurred in the 4 study sites of the western United States were produced using the RTM + TCC method (Fig. 15).

4. Discussion

The RTM + GOS method resulted in high commission errors for the NSV and high omission errors for the SV burnt levels in study site 1. These low accuracies are due to the large number of plots with low TCC, thus the background charcoal and ash contributed more to the reflectance signal, leading to the high commission errors of the NSV burnt level and high omission errors for the SV burnt level. The RTM has the capacity to simulate the canopy reflectance with different TCC levels, and the multi-bands can provide more spectral information to identify different burn severity. Model inversion carried out in a LUT corresponding to a specific TCC level significantly reduced the commission errors in low TCC regions. The overall accuracy and kappa coefficient were significantly improved by integrating TCC in FRT RTM parameterization and backward inversion, but the user's and producer's accuracy of SV and NSV decreased accordingly. These results demonstrated that the spectral confusion between NSV and SV burn severity is inevitable in low TCC regions because of the poor contribution from the photosynthetic vegetation to the signal received by the sensor (Fig. 7a2, 7a3, 7b2, and 7b3). At study site 2, the SV sample (16 plots) was much smaller than NSV (163 plots). Consequently, even the slight commission error in the NSV level markedly influenced the user's accuracy of the SV level and the kappa coefficient. Furthermore, the improvement in accuracy at study site 2 was less than that of study site 1. Our method has demonstrated a potential to reduce the burn severity estimation errors for areas with low TCC, and thus site 1, with lower tree canopy cover than site 2, experienced greater improvement in estimation accuracy. Moreover, the unsatisfactory performance of dNBR and RdNBR also indicated that the empirical methods are limited by field calibration (De Santis et al., 2010; Quintano et al., 2017).

Field surveys were within weeks post-fire at the northern Australia study sites, and were one-year post-fire for western United States study sites. Shortly after a forest fire, the background will contain soil and ash, while one-year post-fire, the understory vegetation will regrow and the charcoal and ash on the soil surface will be removed by rain and wind. Factors such as the degree of recovery of different vegetation strata, soil type and the proportion of surface charcoal will affect the evaluation of burn severity using remotely sensed data. Therefore, assessing burn severity one-year post-fire is much more complicated than doing it immediately post-fire. This suggests that using the same parameterization scheme in all areas is not optimal. This is one of the reasons why the accuracy is not as good as that of previous studies in short-term post-fire burn severity estimation based on RTM methods (RMSE range from 0.14 to 0.21, R^2 range from 0.43 to 0.96) (De Santis et al. 2009, 2010). In some cases, the overestimation errors of low burn severity were largely reduced in the RTM + TCC method but an overestimation was still observed (Fig. 12c) mainly due to a high proportion of charcoal on the soil surface. As shown in Fig. 16, the field CBI values for two field plots from site 5 with low burn severity were 0.15 and 1.12 (Fig. 16). Generally, the proportion of charcoal on the soil surface will decrease dramatically one year after a fire due to rapid

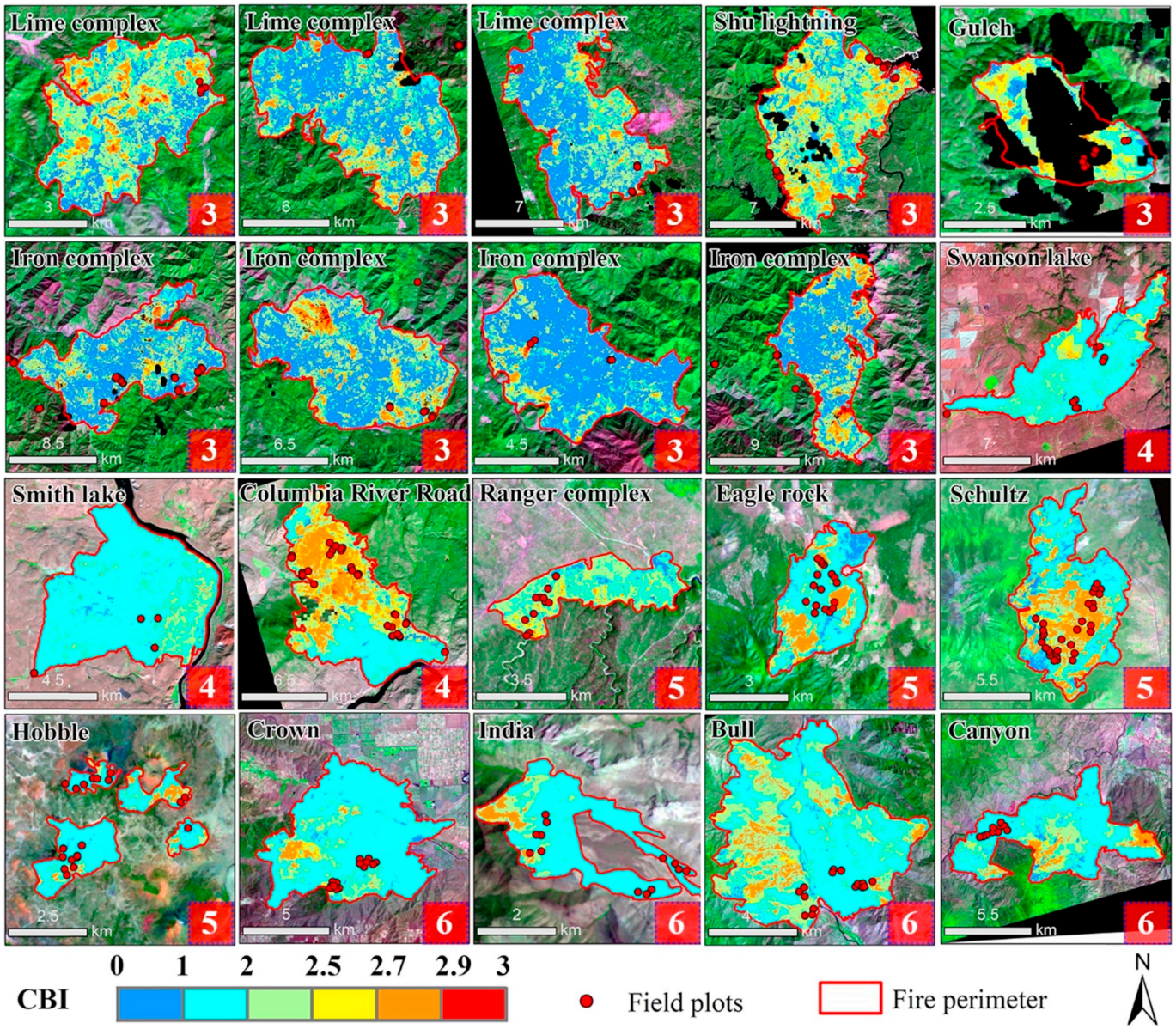

Fig. 15. Burn severity maps based on estimated CBI for 15 fires in the western United States. The background image is a false color composite from a Landsat-5 TM image of each fire region. (For interpretation of the references to color in this figure legend, the reader is referred to the Web version of this article.

vegetation recovery, particularly from low burn severity, but these two field plots are exceptional. The high proportion of charcoal and dead litter on the surface at these two plots greatly influenced the estimation results. That is why our method still overestimated the CBI at these two plots, although it has mitigated most of the estimation error. Overestimation errors are unavoidable in the situation where charcoal still occupies a high proportion of the ground surface one-year post-fire. However, this kind of situation rarely occurs due to the vegetation recovery after fire. Furthermore, even the low CBI in study site 5 (Fig. 12c) was overestimated in this kind of situation, the estimated value was generally lower than 2 and therefore still corresponded to a low burn severity level. In post-fire management, the occurrence of high burn severity areas is generally of greater interest than areas of low burn severity (De Santis et al., 2009). Therefore, the slight overestimation error of low burn severity in this kind of special situation can be tolerated.

5. Conclusions

Burn severity is a critical factor in fire management and in assessing post-fire vegetation recovery. Previous burn severity estimation studies based on RTM simulation methods generally suggest that burn severity and spectral reflectance response have a unique correspondence to each other. However, depending on variations in TCC, background char and ash have different contributions to the spectral signal observed by remote sensors. We found that the same burn severity produced different spectral reflectance values and the same spectral reflectance could be observed from different burn severity levels. In this study, we used a stratified method to integrate TCC into FRT RTM parameterization and backward inversion, to mitigate the spectral confusion between different burn severities under varying TCC. Six study sites across northern Australia and the western United States were selected to validate the proposed method. Compared with the method based on traditional RTM simulation with global optimal search (RTM + GOS), our method (RTM + TCC) significantly reduced the overestimation errors for low burn severity in low TCC regions and underestimation errors for

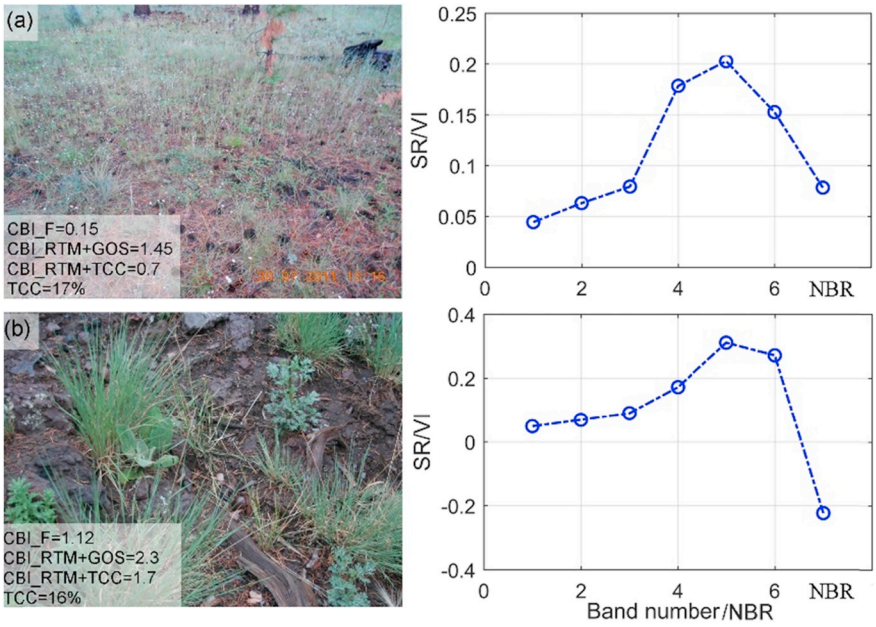

Fig. 16. Photos and corresponding spectrum of two field plots of study site 5 with low burn severity. Photos show that the DCH occupies a big proportion of these two plots and this will lead to an overestimation of burn severity. CBI_F, CBI_RTM + GOS, and CBI_RTM + TCC represent the CBI values of field measurement and estimated based on the RTM + GOS and RTM + TCC methods, respectively.

moderate to high burn severity in high TCC regions. The proposed method also performed better than two commonly used spectral indices, dNBR and RdNBR. Compared with dNBR and RdNBR, the RTM + TCC method is more universal and only requires a single post-fire satellite image, while dNBR and RdNBR require a pair of pre and post-fire satellite images which may be limited in cloudy regions. We also found that the VRE Sentinel-2 bands did not play an important role in burn severity estimation based on full spectral bands and the inversion of FRT RTM. This is probably because other spectral bands or post-fire NBR mask the sensitivity of the VRE bands to fire. The validity of the RTM inversion methods to more accurately classify burn severity in tropical savannas was clearly proven in this study. The greater accuracy of the burn severity mapping estimation resulting from our approach will help us to better understand post-fire vegetation resilience and help in post-fire forest management.

Acknowledgements

This work was supported by the National Natural Science Foundation of China (Contract Nos. 41671361, 41601373 and 41801272), and the Fundamental Research Fund for the Central Universities (Contract No. ZYGX2017KYQD195). We would like to especially thank Prof. Kuusk who provided the code of the latest version of the FRT model, Dr. De Santis who provided the field-measured reflectance of soil, dark charcoal, and light charcoal, and the China Scholarship Council (CSC) for its support of Changming Yin during his scholarship at Australian National University.

References

Addison, P., Oommen, T., 2018. Utilizing satellite radar remote sensing for burn severity estimation. Int. J. Appl. Earth Obs. Geoinf. 73, 292–299.
Bowman, D.M., Balch, J.K., Artaxo, P., Bond, W.J., Carlson, J.M., Cochrane, M.A., D'Antonio, C.M., DeFries, R.S., Doyle, J.C., Harrison, S.P., 2009. Fire in the Earth system. Science 324, 481–484.
Carroll, M., Townshend, J., Hansen, M., DiMiceli, C., Sohlberg, R., Wurster, K., 2010. MODIS vegetative cover conversion and vegetation continuous fields. In: Ramachandran, B., Justice, C.O., Abram, M.J. (Eds.), Land Remote Sensing and Global Environmental Change. Springer, New York, pp. 725–745.
Chuvieco, E., 2009. Global impacts of fire. Earth Observation of Wildland Fires in Mediterranean Ecosystems. Springer, Berlin, pp. 1–10.
Chuvieco, E., Riaño, D., Danson, F., Martin, P., 2006. Use of a radiative transfer model to simulate the postfire spectral response to burn severity. J. Geophys. Res. Biogeo. 111.
Chuvieco, E., Santis, A.d., Riaño, D., Halligan, K., 2007. Simulation approaches for burn severity estimation using remotely sensed images. Fire Ecol. 3 (1), 129–150.
Collins, L., Griffioen, P., Newell, G., Mellor, A., 2018. The utility of random forests for wildfire severity mapping. Remote Sens. Environ. 216, 374–384.
De Santis, A., Asner, G.P., Vaughan, P.J., Knapp, D.E., 2010. Mapping burn severity and burning efficiency in California using simulation models and Landsat imagery. Remote Sens. Environ. 114, 1535–1545.
De Santis, A., Chuvieco, E., 2007. Burn severity estimation from remotely sensed data: performance of simulation versus empirical models. Remote Sens. Environ. 108, 422–435.
De Santis, A., Chuvieco, E., 2009. GeoCBI: a modified version of the Composite Burn Index for the initial assessment of the short-term burn severity from remotely sensed data. Remote Sens. Environ. 113, 554–562.
De Santis, A., Chuvieco, E., Vaughan, P.J., 2009. Short-term assessment of burn severity using the inversion of PROSPECT and GeoSail models. Remote Sens. Environ. 113, 126–136.
Dennison, P.E., Halligan, K.Q., Roberts, D.A., 2004. A comparison of error metrics and constraints for multiple endmember spectral mixture analysis and spectral angle mapper. Remote Sens. Environ. 93, 359–367.
DiMiceli, C., Carroll, M., Sohlberg, R., Huang, C., Hansen, M., Townshend, J., 2011. Annual Global Automated MODIS Vegetation Continuous Fields (MOD44B) at 250 M Spatial Resolution for Data Years Beginning Day 65, 2000–2010, Collection 5 Percent Tree Cover. University of Maryland, College Park, MD, USA.
Edwards, A.C., Maier, S.W., Hutley, L.B., Williams, R.J., Russell-Smith, J., 2013. Spectral analysis of fire severity in north Australian tropical savannas. Remote Sens. Environ. 136, 56–65.
Edwards, A.C., Russell-Smith, J., Maier, S.W., 2018. A comparison and validation of satellite-derived fire severity mapping techniques in fire prone north Australian savannas: extreme fires and tree stem mortality. Remote Sens. Environ. 206, 287–299.
Fernández-Manso, A., Fernández-Manso, O., Quintano, C., 2016a. SENTINEL-2A red-edge spectral indices suitability for discriminating burn severity. Int. J. Appl. Earth Obs. Geoinf. 50, 170–175.
Fernandez-Manso, A., Quintano, C., Roberts, D.A., 2016b. Burn severity influence on post-fire vegetation cover resilience from Landsat MESMA fraction images time series in Mediterranean forest ecosystems. Remote Sens. Environ. 184, 112–123.
Flannigan, M.D., Stocks, B.J., Wotton, B.M., 2000. Climate change and forest fires. Sci. Total Environ. 262, 221–229.
Frolking, S., Palace, M.W., Clark, D., Chambers, J.Q., Shugart, H., Hurtt, G.C., 2009. Forest disturbance and recovery: a general review in the context of spaceborne remote sensing of impacts on aboveground biomass and canopy structure. J. Geophys. Res. Biogeo. 114.
Gascon, F., Bouzinac, C., Thépaut, O., Jung, M., Francesconi, B., Louis, J., Lonjou, V., Lafrance, B., Massera, S., Gaudel-Vacaresse, A., Languille, F., Alhammoud, B., Viallefont, F., Pflug, B., Bieniarz, J., Clerc, S., Pessiot, L., Trémas, T., Cadau, E., De Bonis, R., Isola, C., Martimort, P., Fernandez, V., 2017. Copernicus sentinel-2a calibration and products validation status. Remote Sens. 9, 584.
Gill, A.M., Moore, P.H.R., Williams, R.J., 1996. Fire weather in the wet-dry tropics of the world heritage kakadu national park, Australia. Aust. J. Ecol. 21, 302–308.
Gill, S.J., Biging, G.S., Murphy, E.C., 2000. Modeling conifer tree crown radius and estimating canopy cover. For. Ecol. Manag. 126, 405–416.
Hultquist, C., Chen, G., Zhao, K., 2014. A comparison of Gaussian process regression, random forests and support vector regression for burn severity assessment in diseased forests. Remote Sens. Lett. 5, 723–732.
Jacquemoud, S., Baret, F., 1990. PROSPECT: a model of leaf optical properties spectra. Remote Sens. Environ. 34, 75–91.
Key, C., Benson, N., 2006. Landscape assessment: ground measure of severity, the

Composite Burn Index. In: Lutes, D.C. (Ed.), FIREMON: Fire Effects Monitoring and Inventory System. USDA Forest Service, Rocky Mountain Research Station, Fort Collins, Colorado, USA, pp. LA8–LA15.
Kötz, B., Schaepman, M., Morsdorf, F., Bowyer, P., Itten, K., Allgöwer, B., 2004. Radiative transfer modeling within a heterogeneous canopy for estimation of forest fire fuel properties. Remote Sens. Environ. 92, 332–344.
Kruse, F.A., Lefkoff, A., Boardman, J., Heidebrecht, K., Shapiro, A., Barloon, P., Goetz, A., 1993. The spectral image processing system (SIPS)—interactive visualization and analysis of imaging spectrometer data. Remote Sens. Environ. 44, 145–163.
Kuusk, A., 1995. A Markov chain model of canopy reflectance. Agric. For. Meteorol. 76, 221–236.
Kuusk, A., 2001. A two-layer canopy reflectance model. J. Quant. Spectrosc. Ra. 71, 1–9.
Kuusk, A., Kuusk, J., Lang, M., 2014. Modeling directional forest reflectance with the hybrid type forest reflectance model FRT. Remote Sens. Environ. 149, 196–204.
Kuusk, A., Nilson, T., 2000. A directional multispectral forest reflectance model. Remote Sens. Environ. 72, 244–252.
Kuusk, A., Nilson, T., 2002. Forest reflectance and transmittance FRT user guide. Sci. Chin. D. 41, 580–586.
Lang, M., Nilson, T., Kuusk, A., Kiviste, A., Hordo, M., 2005. The Performance of Different Leaf Mass and Crown Diameter Models in Forming the Input of a Forest Reflectance Model: a Test on Forest Growth Sampleplots and Landsat ETM Images. ForestSat 2005, Boras, Sweden.
Lentile, L.B., Holden, Z.A., Smith, A.M., Falkowski, M.J., Hudak, A.T., Morgan, P., Lewis, S.A., Gessler, P.E., Benson, N.C., 2006. Remote sensing techniques to assess active fire characteristics and post-fire effects. Int. J. Wildland Fire 15, 319–345.
Louis, J., Debaecker, V., Pflug, B., Main-Korn, M., Bieniarz, J., Mueller-Wilm, U., Cadau, E., Gascon, F., 2016. Sentinel-2 Sen2Cor: L2A processor for users. In: Living Planet Symposium, pp. 91.
Main-Knorn, M., Pflug, B., Louis, J., Debaecker, V., Müller-Wilm, U., Gascon, F., 2017. Sen2Cor for sentinel-2. In: Image and Signal Processing for Remote Sensing XXIII. International Society for Optics and Photonics, pp. 1042704.
Masek, J.G., Vermote, E.F., Saleous, N.E., Wolfe, R., Hall, F.G., Huemmrich, K.F., Gao, F., Kutler, J., Lim, T.-K., 2006. A Landsat surface reflectance dataset for North America, 1990–2000. IEEE Geosci. Remote Sens. 3, 68–72.
Mayer, B., Kylling, A., 2005. The libRadtran software package for radiative transfer calculations-description and examples of use. Atmos. Chem. Phys. 5, 1855–1877.
Medhurst, J.L., Beadle, C.L., 2001. Crown structure and leaf area index development in thinned and unthinned *Eucalyptus nitens* plantations. Tree Physiol. 21, 989–999.
Miller, J.D., Knapp, E.E., Key, C.H., Skinner, C.N., Isbell, C.J., Creasy, R.M., Sherlock, J.W., 2009. Calibration and validation of the relative differenced normalized burn ratio (RdNBR) to three measures of fire severity in the sierra Nevada and klamath mountains, California, USA. Remote Sens. Environ. 113, 645–656.
Miller, J.D., Thode, A.E., 2007. Quantifying burn severity in a heterogeneous landscape with a relative version of the delta Normalized Burn Ratio (dNBR). Remote Sens. Environ. 109, 66–80.
Nossent, J., Elsen, P., Bauwens, W., 2011. Sobol' sensitivity analysis of a complex environmental model. Environ. Model. Softw 26, 1515–1525.
O'Grady, A.P., Chen, X., Eamus, D., Hutley, L.B., 2000. Composition, leaf area index and standing biomass of eucalypt open forests near Darwin in the Northern Territory, Australia. Aust. J. Bot. 48, 629–638.
Qiu, S., Zhu, Z., He, B., 2018. Fmask 4.0: improved cloud and cloud shadow detection in Landsats 4-8 and Sentinel-2 imagery. Remote Sens. Environ in review.
Quintano, C., Fernandez-Manso, A., Roberts, D.A., 2017. Burn severity mapping from Landsat MESMA fraction images and land surface temperature. Remote Sens. Environ. 190, 83–95.
Quintano, C., Fernández-Manso, A., Roberts, D.A., 2013. Multiple endmember spectral mixture analysis (MESMA) to map burn severity levels from Landsat images in mediterranean countries. Remote Sens. Environ. 136, 76–88.
Roy, D.P., Boschetti, L., Trigg, S.N., 2006. Remote sensing of fire severity: assessing the performance of the normalized burn ratio. IEEE Geosci. Remote Sens. 3, 112–116.
Sikkink, P.G., Dillon, G.K., Keane, R.E., Morgan, P., Karau, E.C., Holden, Z.A., Silverstein, R.P., 2013. Composite Burn Index (CBI) Data and Field Photos Collected for the FIRESEV Project, Western United States. Forest Service Research Data Archive.
Soverel, N.O., Perrakis, D.D., Coops, N.C., 2010. Estimating burn severity from Landsat dNBR and RdNBR indices across western Canada. Remote Sens. Environ. 114, 1896–1909.
Sprintsin, M., Karnieli, A., Sprintsin, S., Cohen, S., Berliner, P., 2009. Relationships between stand density and canopy structure in a dryland forest as estimated by ground-based measurements and multi-spectral spaceborne images. J. Arid Environ. 73, 955–962.
Sunderman, S.O., Weisberg, P.J., 2011. Remote sensing approaches for reconstructing fire perimeters and burn severity mosaics in desert spring ecosystems. Remote Sens. Environ. 115, 2384–2389.
Wang, J., Li, X., Lu, L., Fang, F., 2013. Parameter sensitivity analysis of crop growth models based on the extended Fourier Amplitude Sensitivity Test method. Environ. Model. Softw 48, 171–182.
Yebra, M., Quan, X., Riaño, D., Larraondo, P.R., van Dijk, A.I., Cary, G.J., 2018. A fuel moisture content and flammability monitoring methodology for continental Australia based on optical remote sensing. Remote Sens. Environ. 212, 260–272.
Zhu, Z., Wang, S., Woodcock, C.E., 2015. Improvement and expansion of the Fmask algorithm: cloud, cloud shadow, and snow detection for Landsats 4–7, 8, and Sentinel 2 images. Remote Sens. Environ. 159, 269–277.
Zhu, Z., Woodcock, C.E., 2012. Object-based cloud and cloud shadow detection in Landsat imagery. Remote Sens. Environ. 118, 83–94.